



Investigation of the p- Σ^0 interaction via femtoscopy in pp collisions

ALICE Collaboration*



ARTICLE INFO

Article history:

Received 16 November 2019
 Received in revised form 27 March 2020
 Accepted 6 April 2020
 Available online 9 April 2020
 Editor: B. Betram

ABSTRACT

This Letter presents the first direct investigation of the p- Σ^0 interaction, using the femtoscopy technique in high-multiplicity pp collisions at $\sqrt{s} = 13$ TeV measured by the ALICE detector. The Σ^0 is reconstructed via the decay channel to $\Lambda\gamma$, and the subsequent decay of Λ to $p\pi^-$. The photon is detected via the conversion in material to e^+e^- pairs exploiting the capability of the ALICE detector to measure electrons at low transverse momenta. The measured p- Σ^0 correlation indicates a shallow strong interaction. The comparison of the data to several theoretical predictions obtained employing the *Correlation Analysis Tool using the Schrödinger Equation* (CATS) and the Lednický-Lyuboshits approach shows that the current experimental precision does not yet allow to discriminate between different models, as it is the case for the available scattering and hypernuclei data. Nevertheless, the p- Σ^0 correlation function is found to be sensitive to the strong interaction, and driven by the interplay of the different spin and isospin channels. This pioneering study demonstrates the feasibility of a femtoscopic measurement in the p- Σ^0 channel and with the expected larger data samples in LHC Run 3 and Run 4, the p- Σ^0 interaction will be constrained with high precision.

© 2020 European Organization for Nuclear Research. Published by Elsevier B.V. This is an open access article under the CC BY license (<http://creativecommons.org/licenses/by/4.0/>). Funded by SCOAP³.

1. Introduction

A quantitative understanding of the hyperon-nucleon interaction in the strangeness $S = -1$ sector is fundamental to pin down the role of strangeness within low energy quantum chromodynamics and to study the properties of baryonic matter at finite densities. The possible presence of the isoscalar Λ and the isovector ($\Sigma^+, \Sigma^0, \Sigma^-$) hyperon states in the inner core of neutron stars (NS) is currently under debate due to the limited knowledge of the interaction of such hyperons with nuclear matter. The inclusion of hyperons in the description of the nuclear matter inside NS typically contains only Λ states, and the on-average attractive nucleon- Λ (N- Λ) interaction leads to rather soft Equations of State (EoS) for NS. These are then unable to provide stability for stars of about two solar masses [1,2]. The Σ hyperons are rarely included in the EoS for NS because of the limited knowledge about the N- Σ strong interaction.

Indeed, while the attractive N- Λ interaction is reasonably well constrained from the available scattering and light hypernuclei data [3–5], the nature of the N- Σ interaction lacks conclusive experimental measurements. One of the major complications for experimental studies is the fact that the decay of all Σ states involves neutral decay products [6], thus requiring high-resolution calorimeters.

The main source of experimental constraints on the N- Σ system comes from scattering measurements [7–9], analysis of Σ^- atoms [10–12], and hypernuclei production data [13–16], although the latter are mainly dominated by large statistical uncertainties and large kaon decay background. Latest hypernuclear results obtained from different nuclear targets point towards an attractive interaction in the isospin $I = 1/2$ channel of the N- Σ system [13,14], and repulsion in the $I = 3/2$ channel [15,16]. Hypernuclear measurements, however, are performed at nuclear saturation density and hence in the presence of more than one nucleon, resulting in a substantial model dependence in the interpretation of the experimental data [17].

Additionally, the hyperon-nucleon dynamics are strongly affected by the conversion process N- $\Lambda \leftrightarrow$ N- Σ , occurring in the $I = 1/2$ channel due to the close kinematic threshold between the two systems (about 80 MeV) [18–22]. This coupling is expected to provide an additional attractive contribution in the two-body N- Λ interaction in vacuum [21,22]. Indeed, depending on the strength of the N- $\Lambda \leftrightarrow$ N- Σ coupling at the two-body level, the corresponding in-medium hyperon properties are very different. For a strong coupling, this leads to a repulsive single-particle potential U_Λ at large densities [21,22]. For the Σ hyperon, the in-medium properties are mostly determined by the overall repulsion in the $I = 3/2$ component [21,22]. A repulsive component in the hyperon-nucleon interactions could shift the onset for hyperon production to larger densities, above 2–3 times the normal saturation density.

* E-mail address: alice-publications@cern.ch.

tion density, thus leading to stiffer EoS which are able to describe the experimental constraint of NS.

To this end, different theoretical approaches including chiral effective field theories (χ EFT) [20] and meson-exchange models with hadronic [23] and quark [24] degrees of freedom provide a similar description of the available data by assuming a strong repulsion in the spin singlet $S = 0$, $I = 1/2$ and spin triplet $S = 1$, $I = 3/2$ and an overall attraction in the remaining channels. Recent ab initio lattice calculations at quark physical masses show a similar dependence on spin-isospin configurations for the central potential term [25]. The strength of the coupled-channel $N-\Lambda \leftrightarrow N-\Sigma$ is strongly model dependent as well. Calculations based on chiral models [20,21] and meson-exchange models [18,26] predict a rather strong or much weaker coupling, respectively. A self-consistent description of this coupled-channel demands a detailed knowledge of the strong interaction in the $N-\Sigma$ system.

Recently, the study of two-particle correlations in momentum space measured in ultra-relativistic proton–proton (pp) and proton–nucleus collisions has proven to provide direct access to the interaction between particle pairs in vacuum [27–29]. The small size of the colliding systems of about 1 fm results in a pronounced correlation signal from strong final state interactions, which permits the latter to be precisely constrained. These measurements provided additional data in the hyperon sector with an unprecedented precision in the low momentum regime. In this Letter, these studies are extended to the Σ sector. The electromagnetic decay of the Σ^0 is exploited for the first direct measurement of the $p-\Sigma^0$ interaction in pp collisions. This study paves the way for extending these investigations to the charged Σ states, in particular in light of the larger data samples expected from the LHC Runs 3 and 4.

2. Data analysis

This Letter presents results obtained from a data sample of pp collisions at $\sqrt{s} = 13$ TeV recorded with the ALICE detector [30,31] during the LHC Run 2 (2015–2018). The sample was collected employing a high-multiplicity trigger with the V0 detectors, which consist of two small-angle plastic scintillator arrays located on either side of the collision vertex at pseudorapidities $2.8 < \eta < 5.1$ and $-3.7 < \eta < -1.7$ [32]. The high-multiplicity trigger is defined by coincident hits in both V0 detectors synchronous with the LHC bunch crossing and by additionally requiring the sum of the measured signal amplitudes in the V0 to exceed a multiple of the average value in minimum bias collisions. This corresponds, at the analysis level, to the highest multiplicity interval containing the top 0.17% of all inelastic collisions with at least one charged particle in $|\eta| < 1$ (referred to as INEL > 0). This data set presents a suitable environment to study correlations due to the enhanced production of strange particles in such collisions [33]. Additionally, the larger charged-particle multiplicity density with respect to the minimum bias sample significantly increases the probability to detect particle pairs. The V0 is also employed to suppress background events, such as the interaction of beam particles with mechanical structures of the beam line, or beam-gas interactions. In-bunch pile-up events with more than one collision per bunch crossing are rejected by evaluating the presence of additional event vertices [31]. The remaining contamination from pile-up events is on the percent level and does not influence the final results.

Charged-particle tracking within the ALICE central barrel is conducted with the Inner Tracking System (ITS) [30] and the Time Projection Chamber (TPC) [34]. The detectors are immersed in a homogeneous 0.5 T solenoidal magnetic field along the beam direction. The ITS consists of six cylindrical layers of high position-resolution silicon detectors placed radially between 3.9 and 43 cm around the beam pipe. The two innermost layers are Silicon Pixel

Detectors (SPD) and cover the pseudorapidity range $|\eta| < 2.0$ and $|\eta| < 1.4$, respectively. The two intermediate layers are composed of Silicon Drift Detectors, and the two outermost layers are made of double-sided Silicon micro-Strip Detectors (SSD), covering $|\eta| < 0.9$ and $|\eta| < 1.0$, respectively. The TPC consists of a 5 m long, cylindrical gaseous detector with full azimuthal coverage in the pseudorapidity range $|\eta| < 0.9$. Particle identification (PID) is conducted via the measurement of the specific ionization energy loss (dE/dx) with up to 159 reconstructed space points along the particle trajectory. The Time-Of-Flight (TOF) [35] detector system is located at a radial distance of 3.7 m from the nominal interaction point and consists of Multigap Resistive Plate Chambers covering the full azimuthal angle in $|\eta| < 0.9$. PID is accomplished by measuring the particle's velocity β via the time of flight of the particles in conjunction with their trajectory. The event collision time is provided as a combination of the measurements in the TOF and the T0 detector, two Cherenkov counter arrays placed at forward rapidity [36].

The primary event vertex (PV) is reconstructed with the combined track information of the ITS and the TPC, and independently with SPD tracklets. When both vertex reconstruction methods are available, the difference of the corresponding z coordinates is required to be smaller than 5 mm. A uniform detector coverage is assured by restricting the maximal deviation between the z coordinate of the reconstructed PV and the nominal interaction point to ± 10 cm. A total of 1.0×10^9 high-multiplicity events are used for the analysis after event selection.

The proton candidates are reconstructed following the analysis methods used for minimum bias pp collisions at $\sqrt{s} = 7$ TeV [27] and 13 TeV [28,29], and are selected from the charged-particle tracks reconstructed with the TPC in the kinematic range $0.5 < p_T < 4.05$ GeV/c and $|\eta| < 0.8$. The TPC and TOF PID capabilities are employed to select proton candidates by the deviation n_σ between the signal hypothesis for a proton and the experimental measurement, normalized by the detector resolution σ . For candidates with $p < 0.75$ GeV/c, PID is performed with the TPC only, requiring $|n_\sigma| < 3$. For larger momenta, the PID information of TPC and TOF are combined. Secondary particles stemming from weak decays or the interaction of primary particles with the detector material contaminate the signal. The corresponding fraction of primary and secondary protons are extracted using Monte Carlo (MC) template fits to the measured distribution of the Distance of Closest Approach (DCA) of the track to the primary vertex [27]. The MC templates are generated using PYTHIA 8.2 [37] and filtered through the ALICE detector [38] and reconstruction algorithm [30]. The resulting purity of protons is found to be 99%, with a primary fraction of 82%.

The Σ^0 is reconstructed via the decay channel $\Sigma^0 \rightarrow \Lambda\gamma$ with a branching ratio of almost 100% [6]. The decay is characterized by a short life time rendering the decay products indistinguishable from primary particles produced in the initial collision. Due to the small mass difference between the Λ and the Σ^0 of about 77 MeV/c 2 , the γ has typically energies of only few hundreds of MeV. Therefore, it is reconstructed relying on conversions to e^+e^- pairs in the detector material of the central barrel exploiting the unique capability of the ALICE detector to identify electrons down to transverse momenta of 0.05 GeV/c. For transverse radii $R < 180$ cm and $|\eta| < 0.9$ the material budget corresponds to $(11.4 \pm 0.5)\%$ of a radiation length X_0 , and accordingly to a conversion probability of $(8.6 \pm 0.4)\%$ [39]. Details of the photon conversion analysis and the corresponding selection criteria are described in [39,40]. The reconstruction relies on the identification of secondary vertices by forming so-called V^0 decay candidates from two oppositely-charged tracks using a procedure described in detail in [41]. The products of the potential γ conversion are reconstructed with the TPC and the ITS in the kinematic range

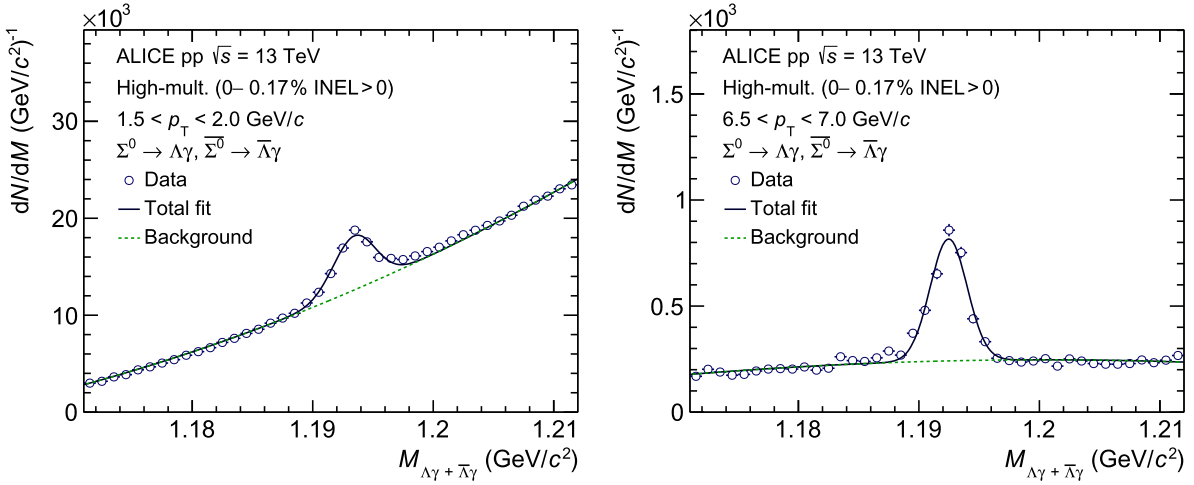


Fig. 1. Invariant mass distribution of the $\Lambda\gamma$ and $\bar{\Lambda}\gamma$ candidates, in two p_T intervals of $1.5 - 2.0 \text{ GeV}/c$ and $6.5 - 7.0 \text{ GeV}/c$. The signal is described by a single Gaussian, and the background by a polynomial of third order. The number of Σ^0 candidates is evaluated within $M_{\Sigma^0}(p_T) \pm 3 \text{ MeV}/c^2$. Only statistical uncertainties are shown.

$p_T > 0.05 \text{ GeV}/c$ and $|\eta| < 0.9$. The candidates for the e^+e^- pair are identified by a broad PID selection in the TPC $-6 < n_\sigma < 7$. The resulting γ candidate is obtained as the combination of the daughter tracks. Only candidates with $p_T > 0.02 \text{ GeV}/c$ and within $|\eta| < 0.9$ are accepted. Combinatorial background from primary e^+e^- pairs, or Dalitz decays of the π^0 and η mesons is removed by requiring that the radial distance of the conversion point, with respect to the detector centre, ranges from 5 cm to 180 cm. Residual contaminations from K_S^0 and Λ are removed by a selection in the Armenteros-Podolanski space [40,42]. Random combinations of electrons and positrons are further suppressed by a two-dimensional selection on the angle between the plane defined by the e^+e^- pair, and the magnetic field [43] in combination with the reduced χ^2 of a refit of the reconstructed V^0 assuming that the particle originates from the primary vertex and has $M_{V^0} = 0$ [40]. The Cosine of the Pointing Angle (CPA) between the γ momentum and the vector pointing from the PV to the decay vertex is required to be $\text{CPA} > 0.999$. In addition to the tight CPA selection, the contribution of particles stemming from out-of-bunch pile-up is suppressed by restricting the DCA of the photon to be along the beam direction ($\text{DCA}_z < 0.5 \text{ cm}$). After application of the selection criteria, about 946×10^6 γ candidates with a purity of about 95.4% are available for further processing.

The Λ particle candidates are reconstructed via the subsequent decay $\Lambda \rightarrow p\pi^-$ with a branching ratio of 63.9% [6], following the procedures described in [27,28]. For the $\bar{\Lambda}$ the charge conjugate decay is exploited, and the same selection criteria are applied. The decay products are reconstructed with the TPC and the ITS within $|\eta| < 0.9$. The daughter candidates are identified by a broad PID selection in the TPC $|n_\sigma| < 5$. The resulting Λ candidate is obtained as the combination of the daughter tracks. The contribution of fake candidates is reduced by requesting a minimum $p_T > 0.3 \text{ GeV}/c$. The coarse PID selection of the daughter tracks introduces a residual K_S^0 contamination in the sample of the Λ candidates. This contamination is removed by a 1.5σ rejection on the invariant mass assuming a decay into $\pi^+\pi^-$, where σ corresponds to the width of a Gaussian fitted to the K_S^0 signal. Topological selections further enhance the purity of the Λ sample. The radial distance of the decay vertex with respect to the detector centre ranges from 0.2 cm to 100 cm and $\text{CPA} > 0.999$. In addition to the tight CPA selection, particles stemming from out-of-bunch pile-up are rejected using the timing information of the SPD and SSD, and the TOF detector. One of the two daughter tracks is required to have a hit in one of these detectors. After application of the selection criteria, about

188×10^6 (178×10^6) Λ ($\bar{\Lambda}$) candidates with a purity of 94.6% (95.3%) are available for further processing.

The Σ^0 ($\bar{\Sigma}^0$) candidates are obtained by combining all Λ ($\bar{\Lambda}$) and γ candidates from the same event, where the nominal particle masses [6] are assumed for the daughters. In particular the timing selection on the daughter tracks of the Λ assures that the Σ^0 candidates stem from the right bunch crossing. In case a daughter track is used to construct two γ , Λ , and $\bar{\Lambda}$ candidates, or a combination thereof, the one with the smaller CPA is removed from the sample. In order to further optimize the yield and the purity of the sample, only Σ^0 candidates with $p_T > 1 \text{ GeV}/c$ are used.

The resulting invariant mass spectrum is shown in Fig. 1 for two p_T intervals. In order to obtain the raw yield, the signal is fitted with a single Gaussian, and the background with a third-order polynomial. Due to the deteriorating momentum resolution for low p_T tracks, the mean value of the Gaussian M_{Σ^0} exhibits a slight p_T dependence, which is well reproduced in MC simulations. The Σ^0 ($\bar{\Sigma}^0$) candidates for femtoscopy are selected as $M_{\Sigma^0}(p_T) \pm 3 \text{ MeV}/c^2$. The width of the interval is chosen as a compromise between the candidate counts and purity. In total, about 115×10^3 (110×10^3) Σ^0 ($\bar{\Sigma}^0$) candidates are found at a purity of about 34.6%. Due to the enhanced combinatorial background at low p_T , the purity increases from about 20% at the lower p_T threshold to its saturation value of about 60% above $5 \text{ GeV}/c$. Only one candidate per event is used, and is randomly selected in the very rare case in which more than one is available. In less than one per mille of the cases when the track of a primary proton is also employed as the daughter track of the γ or the Λ , the corresponding Σ^0 candidate is rejected. Since only strongly decaying resonances feed to the Σ^0 [6], all candidates are considered to be primary particles.

3. Analysis of the correlation function

The experimental definition of the two-particle correlation function, for both p-p and p- Σ^0 pairs, is given by [44],

$$C(k^*) = \mathcal{N} \times \frac{N_{\text{same}}(k^*)}{N_{\text{mixed}}(k^*)} \xrightarrow{k^* \rightarrow \infty} 1, \quad (1)$$

with the same (N_{same}) and mixed (N_{mixed}) event distributions of k^* and a normalization constant \mathcal{N} . The relative momentum of the pair k^* is defined as $k^* = \frac{1}{2} \times |\mathbf{p}_1^* - \mathbf{p}_2^*|$, where \mathbf{p}_1^* and \mathbf{p}_2^* are the momenta of the two particles in the pair rest frame, denoted by the *. The normalization is evaluated in $k^* \in [240, 340] \text{ MeV}/c$ for

p-p and in $k^* \in [250, 400]$ MeV/c for p- Σ^0 pairs, where effects of final state interactions are absent and hence the correlation function approaches unity.

The trajectories of the p-p and \bar{p} - \bar{p} pairs at low k^* are almost collinear, and might therefore be affected by detector effects like track splitting and merging [45]. Accordingly, the reconstruction efficiency for pairs in the same and mixed event might differ. To this end, a close-pair rejection criterion is employed removing p-p and \bar{p} - \bar{p} pairs fulfilling $\sqrt{\Delta\eta^2 + \Delta\varphi^2} < 0.01$, where the azimuthal coordinate φ^* considers the track curvature in the magnetic field.

A total number of 1.7×10^6 (1.3×10^6) p-p (\bar{p} - \bar{p}) and 587 (539) p- Σ^0 (\bar{p} - $\bar{\Sigma}^0$) pairs contribute to the respective correlation function in the region $k^* < 200$ MeV/c. To enhance the statistical significance of the results, the correlation functions of baryon-baryon and antibaryon-antibaryon pairs are combined. Therefore, in the following p- Σ^0 denotes the combination p- $\Sigma^0 \oplus \bar{p}$ - $\bar{\Sigma}^0$, and correspondingly for p-p.

The systematic uncertainties of the experimental correlation function are evaluated by simultaneously varying all proton, Λ , γ , and Σ^0 single-particle selection criteria by up to 20% around the nominal values. Only variations that modify the pair yield by less than 10% (20%) for p- Σ^0 (p-p) with respect to the default choice are considered, and the Σ^0 purity by less than 5%. The impact of statistical fluctuations is reduced by evaluating the systematic uncertainties in intervals of 100 MeV/c (20 MeV/c) in k^* for p- Σ^0 (p-p). The resulting systematic uncertainties are parametrized by an exponential function and interpolated to obtain the final point-by-point uncertainties. At the respectively lowest k^* , the total systematic uncertainties are of the order of 2.5% for both p-p and p- Σ^0 .

Using the femtoscopy formalism [44], the correlation function can be related to the source function $S(r^*)$ and the two-particle wave function $\Psi(\vec{r}^*, \vec{k}^*)$ incorporating the interaction,

$$C(k^*) = \int d^3r^* S(r^*) |\Psi(\vec{r}^*, \vec{k}^*)|^2, \quad (2)$$

where r^* refers to the relative distance between the two particles. As demonstrated in [27–29,46] the correlation function becomes particularly sensitive to the strong interaction for small emission sources formed in pp and p-Pb collisions. For this study, a spherically symmetric emitting source is assumed, with a Gaussian shaped core density profile parametrized by a radius r_0 , which is obtained from a fit to the p-p correlation function, similarly as in [28,29]. Following the premise of a common emission source the such extracted radius is then used as an input to fit the p- Σ^0 correlation function. Possible modifications of the source profile due to the influence of strongly decaying resonances [47–49] are considered in the evaluation of the systematic uncertainties associated with the fitting procedure.

The genuine p-p correlation function is modeled using the *Correlation Analysis Tool using the Schrödinger equation* (CATS) [46], which allows one to use either a local potential $V(r)$ or directly the two-particle wave function, and additionally any source distribution as input to compute the correlation function. For the p-p correlation function the strong Argonne v_{18} potential [50] in the S , P , and D waves is used as an input to CATS.

The theoretical correlation function for p- Σ^0 is modeled employing two different approaches. On the one hand, in CATS the correlation function is computed from the isospin-averaged wave functions obtained within a coupled-channel formalism. On the other hand, the Lednický-Lyuboshits approach [51] relies on the effective-range expansion using scattering parameters as input to evaluate the correlation function. The coupling of the n- Σ^+ system to p- Σ^0 considering the different thresholds is explicitly included by means of a coupled-channel approach, while the effect

Table 1

Weight parameters for the individual components of the measured correlation function. Contributions from feed-down contain the mother particle listed as a sub-index. Non-flat contributions are listed individually.

p-p	p- Σ^0		
Pair	λ parameter (%)	Pair	λ parameter (%)
p-p	67.0	p- Σ^0	22.0
p- Λ -p	20.3	p-($\Lambda\gamma$)	73.1
Feed-down (flat)	11.6	Feed-down (flat)	4.7
Misidentification (flat)	1.1	Misidentification (flat)	0.2

of the p- Λ channel is incorporated by complex scattering parameters [52]. Details of the employed models are described in the next Section.

The experimental data are compared with the modeled correlation function considering the finite experimental momentum resolution [27]. In addition to the genuine correlation function of interest, the measured correlation function also contains residual correlations due to protons coming from weak decays of other particles, such as Λ and Σ^+ (feed-down), and misidentifications. These effects are included by modeling the total correlation function as a decomposition,

$$C_{\text{model}}(k^*) = 1 + \sum_i \lambda_i \times (C_i(k^*) - 1), \quad (3)$$

where the sum runs over all contributions. Their relative contribution is given by the λ parameters computed in a data-driven way from single-particle properties such as the purity and feed-down fractions [27], and are summarized in Table 1.

Apart from the genuine p-p correlation function, a significant contribution comes from the decay of Λ particles feeding to the proton pair. The residual p- Λ correlation function is modeled using either the Usmani potential [53], chiral effective field theory calculations at Leading (LO) [54], or Next-To-Leading order (NLO) [20]. The resulting correlation function is transformed into the momentum basis of the p-p pair by applying the corresponding decay matrices [55]. All other contributions are assumed to be $C(k^*) \sim 1$. Due to the challenging reconstruction of the Σ^0 , the experimental purity of the Σ^0 sample is rather low, and additionally exhibits a strong dependence on the transverse momentum p_T as demonstrated in Fig. 1. The average p_T of the Σ^0 candidates used to construct the correlation function at $k^* < 200$ MeV/c, however, is lower than the $\langle p_T \rangle$ of all inclusive Σ^0 candidates. Considering this effect, the Σ^0 purity employed to compute the λ parameters is found to be 27.4%. Accordingly, the main contribution to the p- Σ^0 correlation function stems from the combinatorial background appearing in the invariant mass spectrum around the Σ^0 peak, which in the following is referred to as $(\Lambda\gamma)$. The shape of the p-($\Lambda\gamma$) correlation function is extracted from the sidebands of the invariant mass selection, and is found to be independent of the choice of mass window. The non-flat behavior is mainly determined by residual p- Λ correlations which are smeared by an uncorrelated γ , and defines the baseline of the measurement of the p- Σ^0 correlation function. The shape is parametrized with a Gaussian distribution and weighted by its λ parameter. All other contributions stemming from misidentified protons or from feed-down are assumed to be $C(k^*) \sim 1$.

The total correlation function including all corrections is then multiplied by a polynomial baseline $C_{\text{non-femto}}(k^*)$,

$$C(k^*) = C_{\text{non-femto}}(k^*) \times C_{\text{model}}(k^*), \quad (4)$$

to account for the normalization and non-femtoscopic background effects stemming e.g. from momentum and energy conservation [27]. The p-p correlation function is fitted in the range

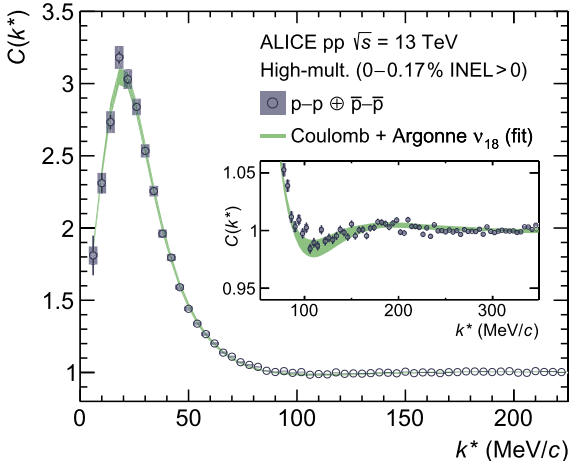


Fig. 2. Measured correlation function of $p-p \oplus \bar{p}-\bar{p}$. Statistical (bars) and systematic uncertainties (boxes) are shown separately. The width of the band corresponds to one standard deviation of the systematic uncertainty of the fit.

$k^* \in [0, 375]$ MeV/c to determine simultaneously the femtoscopic radius r_0 and the parameters of the baseline. To assess the systematic uncertainties on r_0 related to the fitting procedure the upper limit of the fit region is varied within $k^* \in [350, 400]$ MeV/c. The baseline is modeled as a polynomial of zeroth, first, and second order. Additionally, as discussed above, all three models for the $p-\Lambda$ residual correlation function are employed, and the input to the λ parameters is modified by $\pm 20\%$ while maintaining a constant sum of the primary and secondary fractions. The $p-p$ correlation function is shown in Fig. 2, where the width of the bands corresponds to one standard deviation of the total systematic uncertainty of the fit. The inset shows a zoom of the $p-p$ correlation function at intermediate k^* , where the effect of repulsion becomes apparent. The femtoscopic fit yields a radius of $r_0 = 1.249 \pm 0.008$ (stat) $^{+0.024}_{-0.021}$ (syst) fm.

Analyses of $\pi-\pi$ and $K-K$ correlation functions at ultrarelativistic energies in elementary [56] and heavy-ion collisions [57] indicate a source distribution significantly deviating from a Gaussian. Indeed, strongly decaying resonances are known to introduce significant exponential tails to the source distribution, especially for $\pi-\pi$ pairs [47–49]. This becomes evident when studying the corresponding resonance contributions obtained from the statistical hadronization model within the canonical approach [58]. The main resonances feeding to pions, ρ and ω , are significantly longer-lived than those feeding to protons (Δ) and Σ^0 ($\Lambda(1405)$). Hence, it is not surprising that the source distribution for $\pi-\pi$ deviates from a Gaussian. These conclusions are underlined when fitting the $p-p$ correlation function with a Lévy-stable source distribution [59,60]. Leaving both the femtoscopic radius and the stability parameter α for the fit to determine, the Gaussian source shape ($\alpha = 2$) is recovered. Employing a Cauchy-type source distribution ($\alpha = 1$), the data cannot be satisfactorily described. Therefore, the premise of a Gaussian source holds for baryon-baryon pairs.

Accordingly, a Gaussian source with femtoscopic radius r_0 is used to fit the $p-\Sigma^0$ correlation function. The parameters of the linear baseline are obtained from a fit to the $p-(\Lambda\gamma)$ correlation function in $k^* \in [250, 600]$ MeV/c, where it is consistent and kinematically comparable with $p-\Sigma^0$, however featuring significantly smaller uncertainties. The experimental $p-\Sigma^0$ correlation function is then fitted in the range $k^* < 550$ MeV/c, and varied during the fitting procedure within $k^* \in [500, 600]$ MeV/c to determine the systematic uncertainty. Additionally, the input to the λ parameters is modified by $\pm 20\%$ while maintaining a constant sum of the primary and secondary fractions. The parameters of the base-

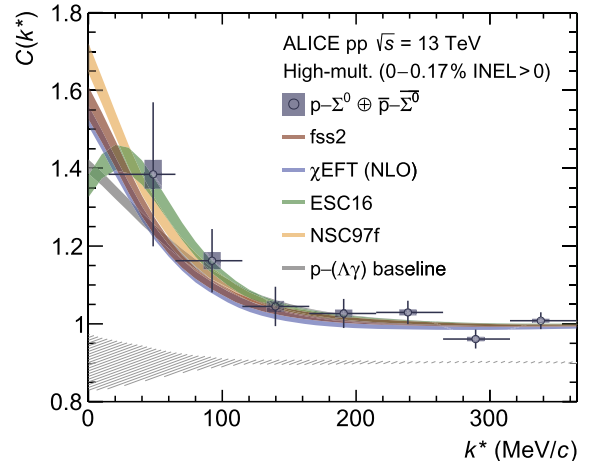


Fig. 3. Measured correlation function of $p-\Sigma^0 \oplus \bar{p}-\bar{\Sigma}^0$. Statistical (bars) and systematic uncertainties (boxes) are shown separately. The gray band denotes the $p-(\Lambda\gamma)$ baseline. The data are compared with different theoretical models. The corresponding correlation functions are computed using CATS [46] for χ EFT [20], NSC97f [26] and ESC16 [23], and using the Lednický-Lyuboshits approach [51,52] for fss2 [24]. The width of the bands corresponds to one standard deviation of the systematic uncertainty of the fit. The absolute correlated uncertainty due to the modeling of the $p-(\Lambda\gamma)$ baseline is shown separately as the hatched area at the bottom of the figure.

line are varied within 1σ of their uncertainties considering their correlation, including the case of a constant baseline. Finally, the femtoscopic radius is varied according to its uncertainties. Possible variations of the $p-\Sigma^0$ source due to contributions of m_T scaling and strong decays are incorporated by decreasing r_0 by 15%, similarly as in [28,29]. The corresponding resonance yields are taken from the statistical hadronization model within the canonical approach [58].

All correlation functions resulting from the above mentioned variations of the selection criteria are fitted during the procedure, additionally considering variations of the mass window to extract the $p-(\Lambda\gamma)$ baseline. The width of the bands in Fig. 3 corresponds to one standard deviation of the total systematic uncertainty of the fit. The absolute correlated uncertainty due to the modeling of the $p-(\Lambda\gamma)$ baseline correlation function is shown separately at the bottom of the figure.

4. Results

The experimental $p-\Sigma^0 \oplus \bar{p}-\bar{\Sigma}^0$ correlation function is shown in Fig. 3. The k^* value of the data points is chosen according to the $\langle k^* \rangle$ of the same event distribution $N_{\text{Same}}(k^*)$ in the corresponding interval. Therefore, due to the low number of counts in the first bin, the data point is shifted with respect to the bin centre. Since the uncertainties of the data are sizable, a direct determination of scattering parameters via a femtoscopic fit is not feasible. Instead, the data are directly compared with the various models of the interaction. These include, on the one hand, meson-exchange models, such as fss2 [24] and two versions of soft-core Nijmegen models (ESC16 [23], NSC97f [61]), and on the other hand results of χ EFT at Next-to-Leading Order (NLO) [20]. The correlation function is modeled using the Lednický-Lyuboshits approach [51] considering the couplings of the $p-\Sigma^0$ system to $p-\Lambda$ and $n-\Sigma^+$ [52] with scattering parameters extracted from the fss2 model. For the case of ESC16, NSC97f and χ EFT, the wave function of the $p-\Sigma^0$ system, including the couplings, is used as an input to CATS to compute the correlation function. The degree of consistency of the data with the discussed models is expressed by the number of standard deviations n_σ , computed in the range $k^* < 150$ MeV/c from the p-value

Table 2

Degree of consistency of the different models with the experimental correlation function.

Model	$p-(\Lambda\gamma)$ baseline	fss2	χ EFT	NSC97f	ESC16
n_σ ($k^* < 150$ MeV/c)	0.2–0.8	0.2–0.9	0.3–1.0	0.2–0.6	0.1–0.5

of the theoretical curves. The range of n_σ shown in Table 2 is computed as one standard deviation of the corresponding distribution. The data are within (0.2–0.8) σ consistent with the $p-(\Lambda\gamma)$ baseline, indicating the presence of an overall shallow strong potential in the $p-\Sigma^0$ channel. The main source of uncertainty of the modeling of the correlation function is the parametrization of the $p-(\Lambda\gamma)$ baseline due the sizeable statistical uncertainties of the latter.

All employed models for the N– Σ interaction potential succeed in reproducing the scattering data in the $S = -1$ sector [7]. Due to the available experimental constraints, the overall description of the $p-\Lambda$ interaction yields a consistent description. On the other hand, the corresponding $p-\Sigma^0$ correlation functions differ significantly among each other. This demonstrates that femtoscopic measurements can discriminate and constrain models, and therefore represent a unique probe to study the N– Σ interaction. Both fss2 and χ EFT exhibit an overall repulsion in N– Σ at intermediate k^* , which mainly occurs in the spin singlet $S = 0$, $I = 1/2$ and spin triplet $S = 1$, $I = 3/2$ components [20,24]. In the low momentum region, below roughly 50 MeV/c, both models yield attraction, which is reflected in the profile of the correlation function. The Nijmegen models, on the other hand, are characterized by a rather constant attraction over the whole range of k^* . In particular at low relative momenta, however, the behavior of the two models deviates significantly. The shape of the correlation function of the most recent Nijmegen model, ESC16, differs significantly from that of the other calculations. This is mainly due to the fact that the occurrence of bound states in the strangeness sector ($S = -1, -2, -3$) is not allowed in the model [23]. This leads to a repulsive core in all the N– Σ channels, which can well be observed in Fig. 3 as the non-monotonic behavior at small relative momenta. In contrast to all other discussed models, NSC97f yields attraction in the spin triplet $S = 1$, $I = 3/2$ channel [61]. Accordingly, the corresponding correlation function demonstrates the strongest attraction at low momenta. The rather large differences among the modeled $p-\Sigma^0$ correlation functions demonstrate that the shape of the latter is very sensitive to details of the strong interaction, and driven by the interplay of the different spin and isospin channels. This shows the strength of femtoscopic measurements, in particular in the N– Σ channel.

The underlying two-body N– Σ interaction obtained within these models, however, translates into significantly different values for the in-medium single-particle potential U_Σ when included in many-body calculations. Both the fss2 quark-model, along with χ EFT, deliver similar results at nuclear saturation density, leading to an overall repulsive U_Σ of around 10–17 MeV [20,21,24]. This is in agreement with evidence from relativistic mean field calculations fitting experimental data of Σ^- atoms [12] and the experimental absence of bound states in Σ hypernuclei [16]. On the contrary, both Nijmegen models yield a slightly attractive Σ single-particle potential, ranging from ≈ -16 MeV for NSC97f to ≈ -3 MeV for ESC16. As already mentioned, however, the interpretation of hypernuclear measurements introduces a significant model dependence. This concerns not only the extraction of the experimental results, relying for instance on the framework of the distorted-wave impulse approximation [17], but also the extrapolation of theoretical calculations to finite density via e.g. the G-matrix approach [62,63].

5. Summary

This Letter presents the first direct investigation of the $p-\Sigma^0$ interaction in high-multiplicity pp collisions at $\sqrt{s} = 13$ TeV, hence proving the feasibility of femtoscopic studies in the N– Σ sector. The $p-\Sigma^0$ correlation function is consistent with the $p-(\Lambda\gamma)$ baseline, and therefore the measurement indicates the presence of an overall shallow strong potential. The data are compared with state-of-the-art descriptions of the interaction, including chiral effective field theory and meson-exchange models. Due to the scarce experimental constraints in the N– Σ sector, the modeled correlation functions differ significantly among each other. The shape of the modeled correlation functions appears to be very sensitive to details of the strong interaction, and is driven by the interplay of the different spin and isospin channels. This proves that femtoscopic measurements in high-energy pp collisions provide a direct study of the genuine two-body N– Σ strong interaction. The presented femtoscopic data cannot discriminate between different models, which is also the case for the available scattering and hypernuclei data.

Further femtoscopic studies enabled by the about two orders of magnitude larger pp data samples of 6 pb^{-1} in minimum bias collisions at $\sqrt{s} = 5.5$ TeV and of 200 pb^{-1} in high-multiplicity at $\sqrt{s} = 14$ TeV, foreseen to be collected in the LHC Runs 3 and 4 [64], will therefore shed light on the N– Σ sector and provide constraints on the models describing the interaction.

Declaration of competing interest

The authors declare that they have no known competing financial interests or personal relationships that could have appeared to influence the work reported in this paper.

Acknowledgements

The ALICE Collaboration is grateful to J. Haidenbauer and T. Rijken for valuable discussions and for providing the theoretical results for the $p-\Sigma^0$ interaction.

The ALICE Collaboration would like to thank all its engineers and technicians for their invaluable contributions to the construction of the experiment and the CERN accelerator teams for the outstanding performance of the LHC complex. The ALICE Collaboration gratefully acknowledges the resources and support provided by all Grid centres and the Worldwide LHC Computing Grid (WLCG) collaboration. The ALICE Collaboration acknowledges the following funding agencies for their support in building and running the ALICE detector: A. I. Alikhanyan National Science Laboratory (Yerevan Physics Institute) Foundation (ANSL), State Committee of Science and World Federation of Scientists (WFS), Armenia; Austrian Academy of Sciences, Austrian Science Fund (FWF): [M 2467-N36] and Nationalstiftung für Forschung, Technologie und Entwicklung, Austria; Ministry of Communications and High Technologies, National Nuclear Research Center, Azerbaijan; Conselho Nacional de Desenvolvimento Científico e Tecnológico (CNPq), Financiadora de Estudos e Projetos (Finep), Fundação de Amparo à Pesquisa do Estado de São Paulo (FAPESP) and Universidade Federal do Rio Grande do Sul (UFRGS), Brazil; Ministry of Education of China (MOEC), Ministry of Science & Technology of China (MSTC) and National Natural Science Foundation of China (NSFC), China; Ministry of Science and Education and Croatian Science Foundation, Croatia; Centro de Aplicaciones Tecnológicas y Desarrollo Nuclear (CEADEN), Cubaenergía, Cuba; Ministry of Education, Youth and Sports of the Czech Republic, Czech Republic; The Danish Council for Independent Research | Natural Sciences, the Villum Fonden and Danish National Research Foundation (DNRF), Denmark; Helsinki Institute of Physics (HIP), Finland; Commissariat à

l'Énergie Atomique (CEA), Institut National de Physique Nucléaire et de Physique des Particules (IN2P3) and Centre National de la Recherche Scientifique (CNRS) and Région des Pays de la Loire, France; Bundesministerium für Bildung und Forschung (BMBF) and GSI Helmholtzzentrum für Schwerionenforschung GmbH, Germany; General Secretariat for Research and Technology, Ministry of Education, Research and Religions, Greece; National Research Development and Innovation Office, Hungary; Department of Atomic Energy, Government of India (DAE), Department of Science and Technology, Government of India (DST), University Grants Commission, Government of India (UGC) and Council of Scientific and Industrial Research (CSIR), India; Indonesian Institute of Sciences, Indonesia; Centro Fermi - Museo Storico della Fisica e Centro Studi e Ricerche Enrico Fermi and Istituto Nazionale di Fisica Nucleare Sezione di Padova (INFN), Italy; Institute for Innovative Science and Technology, Nagasaki Institute of Applied Science (IIIST), Japanese Ministry of Education, Culture, Sports, Science and Technology (MEXT) and Japan Society for the Promotion of Science (JSPS) KAKENHI, Japan; Consejo Nacional de Ciencia (CONACYT) y Tecnología, through Fondo de Cooperación Internacional en Ciencia y Tecnología (FONCICYT) and Dirección General de Asuntos del Personal Académico (DGAPA), Mexico; Nederlandse Organisatie voor Wetenschappelijk Onderzoek (NWO), Netherlands; The Research Council of Norway, Norway; Commission on Science and Technology for Sustainable Development in the South (COMSATS), Pakistan; Pontificia Universidad Católica del Perú, Peru; Ministry of Science and Higher Education and National Science Centre, Poland; Korea Institute of Science and Technology Information and National Research Foundation of Korea (NRF), Republic of Korea; Ministry of Education and Scientific Research, Institute of Atomic Physics and Ministry of Research and Innovation and Institute of Atomic Physics, Romania; Joint Institute for Nuclear Research (JINR), Ministry of Education and Science of the Russian Federation, National Research Centre Kurchatov Institute, Russian Science Foundation and Russian Foundation for Basic Research, Russia; Ministry of Education, Science, Research and Sport of the Slovak Republic, Slovakia; National Research Foundation of South Africa, South Africa; Swedish Research Council (VR) and Knut & Alice Wallenberg Foundation (KAW), Sweden; European Organization for Nuclear Research, Switzerland; Suranaree University of Technology (SUT), National Science and Technology Development Agency (NSDTA) and Office of the Higher Education Commission under NRU project of Thailand, Thailand; Turkish Atomic Energy Agency (TAEK), Turkey; National Academy of Sciences of Ukraine, Ukraine; Science and Technology Facilities Council (STFC), United Kingdom; National Science Foundation of the United States of America (NSF) and United States Department of Energy, Office of Nuclear Physics (DOE NP), United States of America.

References

- [1] P. Demorest, T. Pennucci, S. Ransom, M. Roberts, J. Hessels, Shapiro delay measurement of a two solar mass neutron star, *Nature* 467 (2010) 1081–1083.
- [2] J. Antoniadis, et al., A massive pulsar in a compact relativistic binary, *Science* 340 (2013) 6131.
- [3] G. Alexander, et al., Study of the $\Lambda - n$ system in low-energy $\Lambda - p$ elastic scattering, *Phys. Rev.* 173 (1968) 1452–1460.
- [4] B. Sechi-Zorn, B. Kehoe, J. Twitty, R.A. Burnstein, Low-energy Λ -proton elastic scattering, *Phys. Rev.* 175 (1968) 1735–1740.
- [5] O. Hashimoto, H. Tamura, Spectroscopy of Λ hypernuclei, *Prog. Part. Nucl. Phys.* 57 (2006) 564–653.
- [6] Particle Data Group Collaboration, M. Tanabashi, et al., Review of particle physics, *Phys. Rev. D* 98 (2018) 030001.
- [7] F. Eisele, H. Filthuth, W. Foehlisch, V. Hepp, G. Zech, Elastic $\Sigma^+ - p$ scattering at low energies, *Phys. Lett. B* 37 (1971) 204–206.
- [8] R. Engelmann, H. Filthuth, V. Hepp, E. Kluge, Inelastic $\Sigma^- p$ -interactions at low momenta, *Phys. Lett. B* 21 (1966) 587–589.
- [9] V. Hepp, H. Schleich, A new determination of the capture ratio $r(c) = \Sigma^- p \rightarrow \Sigma^0 n / ((\Sigma^- p \rightarrow \Sigma^0 n) + (\Sigma^- p \rightarrow \Lambda n))$, the Λ^0 -lifetime and $\Sigma^- \Lambda^0$ mass difference, *Z. Phys.* 214 (1968) 71.
- [10] C. Batty, E. Friedman, A. Gal, Density dependence of the Σ nucleus optical potential derived from Σ^- atom data, *Phys. Lett. B* 335 (1994) 273–278.
- [11] C.J. Batty, E. Friedman, A. Gal, Density dependence in Σ^- atoms and implications for Σ hypernuclei, *Prog. Theor. Phys. Suppl.* 117 (1994) 227–240.
- [12] J. Mares, E. Friedman, A. Gal, B.K. Jennings, Constraints on Σ nucleus dynamics from Dirac phenomenology of Σ^- atoms, *Nucl. Phys. A* 594 (1995) 311–324.
- [13] R.S. Hayano, et al., Observation of a bound state of ${}^4_\Sigma$ He hypernucleus, *Phys. Lett. B* 231 (1989) 355–358.
- [14] T. Nagae, et al., Observation of a ${}^4_\Sigma$ He bound state in the ${}^4\text{He}(K^-, \pi^-)$ reaction at 600 MeV/c, *Phys. Rev. Lett.* 80 (1998) 1605–1609.
- [15] L. Tang, et al., Observations of hyperon-nucleus systems produced on ${}^{12}\text{C}$ and ${}^7\text{Li}$ targets using the (K^-, π^+) reaction at 715 MeV/c, *Phys. Rev. C* 38 (1988) 846–853.
- [16] P.K. Saha, et al., Study of the Σ -nucleus potential by the (π^-, K^+) reaction on medium-to-heavy nuclear targets, *Phys. Rev. C* 70 (2004) 044613.
- [17] A. Gal, E.V. Hungerford, D.J. Millener, Strangeness in nuclear physics, *Rev. Mod. Phys.* 88 (2016) 035004.
- [18] J. Haidenbauer, U.-G. Meißner, Jülich hyperon-nucleon model revisited, *Phys. Rev. C* 72 (2005) 044005.
- [19] T.A. Rijken, M.M. Nagels, Y. Yamamoto, Baryon-baryon interactions: Nijmegen extended-soft-core models, *Prog. Theor. Phys. Suppl.* 185 (2010) 14–71.
- [20] J. Haidenbauer, S. Petschauer, N. Kaiser, U.G. Meißner, A. Nogga, W. Weise, Hyperon-nucleon interaction at next-to-leading order in chiral effective field theory, *Nucl. Phys. A* 915 (2013) 24–58.
- [21] J. Haidenbauer, U.G. Meißner, A. Nogga, Hyperon-nucleon interaction within chiral effective field theory revisited, arXiv:1906.11681 [nucl-th].
- [22] J. Haidenbauer, U.G. Meißner, N. Kaiser, W. Weise, Lambda-nuclear interactions and hyperon puzzle in neutron stars, *Eur. Phys. J. A* 53 (2017) 121.
- [23] M.M. Nagels, T.A. Rijken, Y. Yamamoto, Extended-soft-core baryon-baryon model ESC16. II. Hyperon-nucleon interactions, *Phys. Rev. C* 99 (2019) 044003.
- [24] Y. Fujiwara, Y. Suzuki, C. Nakamoto, Baryon-baryon interactions in the SU(6) quark model and their applications to light nuclear systems, *Prog. Part. Nucl. Phys.* 58 (2007) 439–520.
- [25] H. Nemura, et al., Baryon interactions from lattice QCD with physical masses – strangeness $S = -1$ sector, *EPJ Web Conf.* 175 (2018) 05030.
- [26] T.A. Rijken, V.G.J. Stoks, Y. Yamamoto, Soft core hyperon-nucleon potentials, *Phys. Rev. C* 59 (1999) 21–40.
- [27] ALICE Collaboration, S. Acharya, et al., p - p , p - Λ and Λ - Λ correlations studied via femtoscopy in pp reactions at $\sqrt{s} = 7$ TeV, *Phys. Rev. C* 99 (2019) 024001.
- [28] ALICE Collaboration, S. Acharya, et al., Study of the Λ - Λ interaction with femtoscopy correlations in pp and p - Pb collisions at the LHC, *Phys. Lett. B* 797 (2019) 134822.
- [29] ALICE Collaboration, S. Acharya, et al., First observation of an attractive interaction between a proton and a multi-strange baryon, *Phys. Rev. Lett.* 123 (2019) 112002.
- [30] ALICE Collaboration, K. Aamodt, et al., The ALICE experiment at the CERN LHC, *J. Instrum.* 3 (2008) S08002.
- [31] ALICE Collaboration, B. Abelev, et al., Performance of the ALICE experiment at the CERN LHC, *Int. J. Mod. Phys. A* 29 (2014) 1430044.
- [32] ALICE Collaboration, E. Abbas, et al., Performance of the ALICE VZERO system, *J. Instrum.* 8 (2013) P10016.
- [33] ALICE Collaboration, J. Adam, et al., Enhanced production of multi-strange hadrons in high-multiplicity proton-proton collisions, *Nat. Phys.* 13 (2017) 535–539.
- [34] J. Alme, et al., The ALICE TPC, a large 3-dimensional tracking device with fast readout for ultra-high multiplicity events, *Nucl. Instrum. Methods A* 622 (2010) 316–367.
- [35] A. Akindinov, et al., Performance of the ALICE time-of-flight detector at the LHC, *Eur. Phys. J. Plus* 128 (2013) 44.
- [36] ALICE Collaboration, J. Adam, et al., Determination of the event collision time with the ALICE detector at the LHC, *Eur. Phys. J. Plus* 132 (2017) 99.
- [37] T. Sjöstrand, et al., An introduction to PYTHIA 8.2, *Comput. Phys. Commun.* 191 (2015) 159–177.
- [38] R. Brun, F. Bruyant, M. Maire, A.C. McPherson, P. Zanarini, GEANT 3: User's Guide Geant 3.10, Geant 3.11; rev. version, CERN, Geneva, 1987.
- [39] ALICE Collaboration, B. Abelev, et al., Neutral pion and η meson production in proton-proton collisions at $\sqrt{s} = 0.9$ TeV and $\sqrt{s} = 7$ TeV, *Phys. Lett. B* 717 (2012) 162–172.
- [40] ALICE Collaboration, S. Acharya, et al., Neutral pion and η meson production in p - Pb collisions at $\sqrt{s_{\text{NN}}} = 5.02$ TeV, *Eur. Phys. J. C* 78 (2018) 624.
- [41] ALICE Collaboration, B. Alessandro, et al., ALICE: physics performance report, volume II, *J. Phys. G* 32 (2006) 1295.
- [42] J. Podolanski, R. Armenteros, III. Analysis of V-events, *Philos. Mag.* 45 (1954) 13–30.
- [43] PHENIX Collaboration, A. Adare, et al., Detailed measurement of the e^+e^- pair continuum in $p + p$ and $\text{Au} + \text{Au}$ collisions at $\sqrt{s_{\text{NN}}} = 200$ GeV and implications for direct photon production, *Phys. Rev. C* 81 (2010) 034911.
- [44] M.A. Lisa, S. Pratt, R. Soltz, U. Wiedemann, Femtoscopy in relativistic heavy ion collisions, *Annu. Rev. Nucl. Part. Sci.* 55 (2005) 357–402.

- [45] ALICE Collaboration, J. Adam, et al., One-dimensional pion, kaon, and proton femtoscopy in Pb-Pb collisions at $\sqrt{s_{NN}} = 2.76$ TeV, Phys. Rev. C 92 (2015) 054908.
- [46] D.L. Mihaylov, V. Mantovani Sarti, O.W. Arnold, L. Fabbietti, B. Hohlweger, A.M. Mathis, A femtoscopic correlation analysis tool using the Schrödinger equation (CATS), Eur. Phys. J. C 78 (2018) 394.
- [47] U.A. Wiedemann, U. Heinz, New class of Hanbury-Brown-Twiss parameters, Phys. Rev. C 56 (1997) R610–R613.
- [48] U.A. Wiedemann, U.W. Heinz, Resonance contributions to HBT correlation radii, Phys. Rev. C 56 (1997) 3265–3286.
- [49] A. Kisiel, W. Florkowski, W. Broniowski, Femtoscopy in hydro-inspired models with resonances, Phys. Rev. C 73 (2006) 064902.
- [50] R.B. Wiringa, V.G.J. Stoks, R. Schiavilla, An accurate nucleon-nucleon potential with charge independence breaking, Phys. Rev. C 51 (1995) 38–51.
- [51] R. Lednický, V.I. Lyuboshits, Final state interaction effect on pairing correlations between particles with small relative momenta, Sov. J. Nucl. Phys. 35 (1982) 770.
- [52] A. Stavinskij, K. Mikhailov, B. Erazmus, R. Lednický, Residual correlations between decay products of $\pi^0\pi^0$ and $p\Sigma^0$ systems, arXiv:0704.3290 [nucl-th].
- [53] A.R. Bodmer, Q.N. Usmani, J. Carlson, Binding energies of hypernuclei and three-body ΔNN forces, Phys. Rev. C 29 (1984) 684–687.
- [54] H. Polinder, J. Haidenbauer, U.-G. Meißner, Hyperon-nucleon interactions – a chiral effective field theory approach, Nucl. Phys. A 779 (2006) 244–266.
- [55] A. Kisiel, H. Zbroszczyk, M. Szymański, Extracting baryon-antibaryon strong-interaction potentials from $p\bar{A}$ femtoscopic correlation functions, Phys. Rev. C 89 (2014) 054916.
- [56] CMS Collaboration, A.M. Sirunyan, et al., Bose-Einstein correlations in pp , pPb , and $PbPb$ collisions at $\sqrt{s_{NN}} = 0.9 - 7$ TeV, Phys. Rev. C 97 (2018) 064912.
- [57] PHENIX Collaboration, A. Adare, et al., Lévy-stable two-pion Bose-Einstein correlations in $\sqrt{s_{NN}} = 200$ GeV Au + Au collisions, Phys. Rev. C 97 (2018) 064911.
- [58] F. Becattini, P. Castorina, A. Milov, H. Satz, Predictions of hadron abundances in pp collisions at the LHC, J. Phys. G 38 (2011) 025002.
- [59] T. Csörgő, S. Hegyi, W.A. Zajc, Bose-Einstein correlations for Lévy stable source distributions, Eur. Phys. J. C 36 (2004) 67.
- [60] R. Metzler, E. Barkai, J. Klafter, Anomalous diffusion and relaxation close to thermal equilibrium: a fractional Fokker-Planck equation approach, Phys. Rev. Lett. 82 (1999) 3563.
- [61] T.A. Rijken, V.G.J. Stoks, Y. Yamamoto, Soft-core hyperon-nucleon potentials, Phys. Rev. C 59 (1999) 21–40.
- [62] Y. Yamamoto, T. Motoba, H. Himeno, K. Ikeda, S. Nagata, Hyperon nucleon and hyperon-hyperon interactions in nuclei, Prog. Theor. Phys. Suppl. 117 (1994) 361–389.
- [63] Y. Yamamoto, T. Motoba, T.A. Rijken, G-matrix approach to hyperon-nucleus systems, Prog. Theor. Phys. Suppl. 185 (2010) 72–105.
- [64] ALICE Collaboration, S. Acharya, et al., ALICE upgrade physics performance studies for 2018 report on HL/HE-LHC physics, <https://cds.cern.ch/record/2661798>.

ALICE Collaboration

S. Acharya ¹⁴¹, D. Adamová ⁹⁴, A. Adler ⁷⁴, J. Adolfsson ⁸⁰, M.M. Aggarwal ⁹⁹, G. Aglieri Rinella ³³, M. Agnello ³⁰, N. Agrawal ^{10,53}, Z. Ahammed ¹⁴¹, S. Ahmad ¹⁶, S.U. Ahn ⁷⁶, A. Akindinov ⁹¹, M. Al-Turany ¹⁰⁶, S.N. Alam ¹⁴¹, D.S.D. Albuquerque ¹²², D. Aleksandrov ⁸⁷, B. Alessandro ⁵⁸, H.M. Alfanda ⁶, R. Alfaro Molina ⁷¹, B. Ali ¹⁶, Y. Ali ¹⁴, A. Alici ^{10,26,53}, A. Alkin ², J. Alme ²¹, T. Alt ⁶⁸, L. Altenkamper ²¹, I. Altsybeev ¹¹², M.N. Anaam ⁶, C. Andrei ⁴⁷, D. Andreou ³³, H.A. Andrews ¹¹⁰, A. Andronic ¹⁴⁴, M. Angeletti ³³, V. Anguelov ¹⁰³, C. Anson ¹⁵, T. Antičić ¹⁰⁷, F. Antinori ⁵⁶, P. Antonioli ⁵³, R. Anwar ¹²⁵, N. Apadula ⁷⁹, L. Aphectche ¹¹⁴, H. Appelshäuser ⁶⁸, S. Arcelli ²⁶, R. Arnaldi ⁵⁸, M. Arratia ⁷⁹, I.C. Arsene ²⁰, M. Arslanbekci ¹⁰³, A. Augustinus ³³, R. Averbeck ¹⁰⁶, S. Aziz ⁶¹, M.D. Azmi ¹⁶, A. Badalà ⁵⁵, Y.W. Baek ⁴⁰, S. Bagnasco ⁵⁸, X. Bai ¹⁰⁶, R. Bailhache ⁶⁸, R. Bala ¹⁰⁰, A. Baldissari ¹³⁷, M. Ball ⁴², S. Balouza ¹⁰⁴, R. Barbera ²⁷, L. Barioglio ²⁵, G.G. Barnaföldi ¹⁴⁵, L.S. Barnby ⁹³, V. Barret ¹³⁴, P. Bartalini ⁶, K. Barth ³³, E. Bartsch ⁶⁸, F. Baruffaldi ²⁸, N. Bastid ¹³⁴, S. Basu ¹⁴³, G. Batigne ¹¹⁴, B. Batyunya ⁷⁵, D. Bauri ⁴⁸, J.L. Bazo Alba ¹¹¹, I.G. Bearden ⁸⁸, C. Bedda ⁶³, N.K. Behera ⁶⁰, I. Belikov ¹³⁶, A.D.C. Bell Hechavarria ¹⁴⁴, F. Bellini ³³, R. Bellwied ¹²⁵, V. Belyaev ⁹², G. Bencedi ¹⁴⁵, S. Beole ²⁵, A. Bercuci ⁴⁷, Y. Berdnikov ⁹⁷, D. Berenyi ¹⁴⁵, R.A. Bertens ¹³⁰, D. Berziano ⁵⁸, M.G. Besoiu ⁶⁷, L. Betev ³³, A. Bhasin ¹⁰⁰, I.R. Bhat ¹⁰⁰, M.A. Bhat ³, H. Bhatt ⁴⁸, B. Bhattacharjee ⁴¹, A. Bianchi ²⁵, L. Bianchi ²⁵, N. Bianchi ⁵¹, J. Bielčík ³⁶, J. Bielčíková ⁹⁴, A. Bilandžić ^{104,117}, G. Biro ¹⁴⁵, R. Biswas ³, S. Biswas ³, J.T. Blair ¹¹⁹, D. Blau ⁸⁷, C. Blume ⁶⁸, G. Boca ¹³⁹, F. Bock ^{33,95}, A. Bogdanov ⁹², S. Boi ²³, L. Boldizsár ¹⁴⁵, A. Bolozdynya ⁹², M. Bomba ³⁷, G. Bonomi ¹⁴⁰, H. Borel ¹³⁷, A. Borissov ^{92,144}, H. Bossi ¹⁴⁶, E. Botta ²⁵, L. Bratrud ⁶⁸, P. Braun-Munzinger ¹⁰⁶, M. Bregant ¹²¹, M. Broz ³⁶, E.J. Brucken ⁴³, E. Bruna ⁵⁸, G.E. Bruno ¹⁰⁵, M.D. Buckland ¹²⁷, D. Budnikov ¹⁰⁸, H. Buesching ⁶⁸, S. Bufalino ³⁰, O. Bugnon ¹¹⁴, P. Buhler ¹¹³, P. Buncic ³³, Z. Buthelezi ^{72,131}, J.B. Butt ¹⁴, J.T. Buxton ⁹⁶, S.A. Bysiak ¹¹⁸, D. Caffarri ⁸⁹, A. Caliva ¹⁰⁶, E. Calvo Villar ¹¹¹, R.S. Camacho ⁴⁴, P. Camerini ²⁴, A.A. Capon ¹¹³, F. Carnesecchi ^{10,26}, R. Caron ¹³⁷, J. Castillo Castellanos ¹³⁷, A.J. Castro ¹³⁰, E.A.R. Casula ⁵⁴, F. Catalano ³⁰, C. Ceballos Sanchez ⁵², P. Chakraborty ⁴⁸, S. Chandra ¹⁴¹, W. Chang ⁶, S. Chapeland ³³, M. Chartier ¹²⁷, S. Chattopadhyay ¹⁴¹, S. Chattpadhyay ¹⁰⁹, A. Chauvin ²³, C. Cheshkov ¹³⁵, B. Cheynis ¹³⁵, V. Chibante Barroso ³³, D.D. Chinellato ¹²², S. Cho ⁶⁰, P. Chochula ³³, T. Chowdhury ¹³⁴, P. Christakoglou ⁸⁹, C.H. Christensen ⁸⁸, P. Christiansen ⁸⁰, T. Chujo ¹³³, C. Cicalo ⁵⁴, L. Cifarelli ^{10,26}, F. Cindolo ⁵³, J. Cleymans ¹²⁴, F. Colamaria ⁵², D. Colella ⁵², A. Collu ⁷⁹, M. Colocci ²⁶, M. Concias ^{58,ii}, G. Conesa Balbastre ⁷⁸, Z. Conesa del Valle ⁶¹, G. Contin ^{24,127}, J.G. Contreras ³⁶, T.M. Cormier ⁹⁵, Y. Corrales Morales ²⁵, P. Cortese ³¹, M.R. Cosentino ¹²³, F. Costa ³³, S. Costanza ¹³⁹, P. Crochet ¹³⁴, E. Cuautle ⁶⁹, P. Cui ⁶, L. Cunqueiro ⁹⁵, D. Dabrowski ¹⁴², T. Dahms ^{104,117}, A. Dainese ⁵⁶, F.P.A. Damas ^{114,137}, M.C. Danisch ¹⁰³, A. Danu ⁶⁷, D. Das ¹⁰⁹, I. Das ¹⁰⁹, P. Das ⁸⁵, P. Das ³, S. Das ³, A. Dash ⁸⁵, S. Dash ⁴⁸, S. De ⁸⁵, A. De Caro ²⁹, G. de Cataldo ⁵², J. de Cuveland ³⁸, A. De Falco ²³, D. De Gruttola ¹⁰, N. De Marco ⁵⁸, S. De Pasquale ²⁹, S. Deb ⁴⁹, B. Debjani ³, H.F. Degenhardt ¹²¹,

- K.R. Deja ¹⁴², A. Deloff ⁸⁴, S. Delsanto ^{25,131}, D. Devetak ¹⁰⁶, P. Dhankher ⁴⁸, D. Di Bari ³², A. Di Mauro ³³, R.A. Diaz ⁸, T. Dietel ¹²⁴, P. Dillenseger ⁶⁸, Y. Ding ⁶, R. Divià ³³, D.U. Dixit ¹⁹, Ø. Djurvsland ²¹, U. Dmitrieva ⁶², A. Dobrin ^{33,67}, B. Dönigus ⁶⁸, O. Dordic ²⁰, A.K. Dubey ¹⁴¹, A. Dubla ¹⁰⁶, S. Dudi ⁹⁹, M. Dukhishyam ⁸⁵, P. Dupieux ¹³⁴, R.J. Ehlers ¹⁴⁶, V.N. Eikeland ²¹, D. Elia ⁵², H. Engel ⁷⁴, E. Epple ¹⁴⁶, B. Erazmus ¹¹⁴, F. Erhardt ⁹⁸, A. Erokhin ¹¹², M.R. Ersdal ²¹, B. Espagnon ⁶¹, G. Eulisse ³³, D. Evans ¹¹⁰, S. Evdokimov ⁹⁰, L. Fabbietti ^{104,117}, M. Faggin ²⁸, J. Faivre ⁷⁸, F. Fan ⁶, A. Fantoni ⁵¹, M. Fasel ⁹⁵, P. Fecchio ³⁰, A. Feliciello ⁵⁸, G. Feofilov ¹¹², A. Fernández Téllez ⁴⁴, A. Ferrero ¹³⁷, A. Ferretti ²⁵, A. Festanti ³³, V.J.G. Feuillard ¹⁰³, J. Figiel ¹¹⁸, S. Filchagin ¹⁰⁸, D. Finogeev ⁶², F.M. Fionda ²¹, G. Fiorenza ⁵², F. Flor ¹²⁵, S. Foertsch ⁷², P. Foka ¹⁰⁶, S. Fokin ⁸⁷, E. Fragiocomo ⁵⁹, U. Frankenfeld ¹⁰⁶, U. Fuchs ³³, C. Furget ⁷⁸, A. Furs ⁶², M. Fusco Girard ²⁹, J.J. Gaardhøje ⁸⁸, M. Gagliardi ²⁵, A.M. Gago ¹¹¹, A. Gal ¹³⁶, C.D. Galvan ¹²⁰, P. Ganoti ⁸³, C. Garabatos ¹⁰⁶, E. Garcia-Solis ¹¹, K. Garg ²⁷, C. Gargiulo ³³, A. Garibli ⁸⁶, K. Garner ¹⁴⁴, P. Gasik ^{104,117}, E.F. Gauger ¹¹⁹, M.B. Gay Ducati ⁷⁰, M. Germain ¹¹⁴, J. Ghosh ¹⁰⁹, P. Ghosh ¹⁴¹, S.K. Ghosh ³, P. Gianotti ⁵¹, P. Giubellino ^{58,106}, P. Giubilato ²⁸, P. Glässel ¹⁰³, D.M. Goméz Coral ⁷¹, A. Gomez Ramirez ⁷⁴, V. Gonzalez ¹⁰⁶, P. González-Zamora ⁴⁴, S. Gorbunov ³⁸, L. Görlich ¹¹⁸, S. Gotovac ³⁴, V. Grabski ⁷¹, L.K. Graczykowski ¹⁴², K.L. Graham ¹¹⁰, L. Greiner ⁷⁹, A. Grelli ⁶³, C. Grigoras ³³, V. Grigoriev ⁹², A. Grigoryan ¹, S. Grigoryan ⁷⁵, O.S. Groettvik ²¹, F. Grossa ³⁰, J.F. Grosse-Oetringhaus ³³, R. Grossi ¹⁰⁶, R. Guernane ⁷⁸, M. Guittiere ¹¹⁴, K. Gulbrandsen ⁸⁸, T. Gunji ¹³², A. Gupta ¹⁰⁰, R. Gupta ¹⁰⁰, I.B. Guzman ⁴⁴, R. Haake ¹⁴⁶, M.K. Habib ¹⁰⁶, C. Hadjidakis ⁶¹, H. Hamagaki ⁸¹, G. Hamar ¹⁴⁵, M. Hamid ⁶, R. Hannigan ¹¹⁹, M.R. Haque ^{63,85}, A. Harlenderova ¹⁰⁶, J.W. Harris ¹⁴⁶, A. Harton ¹¹, J.A. Hasenbichler ³³, H. Hassan ⁹⁵, D. Hatzifotiadou ^{10,53}, P. Hauer ⁴², S. Hayashi ¹³², S.T. Heckel ^{68,104}, E. Hellbär ⁶⁸, H. Helstrup ³⁵, A. Herghelegiu ⁴⁷, T. Herman ³⁶, E.G. Hernandez ⁴⁴, G. Herrera Corral ¹⁹, F. Herrmann ¹⁴⁴, K.F. Hetland ³⁵, T.E. Hilden ⁴³, H. Hillemanns ³³, C. Hills ¹²⁷, B. Hippolyte ¹³⁶, B. Hohlweyer ¹⁰⁴, D. Horak ³⁶, A. Hornung ⁶⁸, S. Hornung ¹⁰⁶, R. Hosokawa ^{15,133}, P. Hristov ³³, C. Huang ⁶¹, C. Hughes ¹³⁰, P. Huhn ⁶⁸, T.J. Humanic ⁹⁶, H. Hushnud ¹⁰⁹, L.A. Husova ¹⁴⁴, N. Hussain ⁴¹, S.A. Hussain ¹⁴, D. Hutter ³⁸, J.P. Iddon ^{33,127}, R. Ilkaev ¹⁰⁸, M. Inaba ¹³³, G.M. Innocenti ³³, M. Ippolitov ⁸⁷, A. Isakov ⁹⁴, M.S. Islam ¹⁰⁹, M. Ivanov ¹⁰⁶, V. Ivanov ⁹⁷, V. Izucheev ⁹⁰, B. Jacak ⁷⁹, N. Jacazio ⁵³, P.M. Jacobs ⁷⁹, S. Jadlovska ¹¹⁶, J. Jadlovsky ¹¹⁶, S. Jaelani ⁶³, C. Jahnke ¹²¹, M.J. Jakubowska ¹⁴², M.A. Janik ¹⁴², T. Janson ⁷⁴, M. Jercic ⁹⁸, O. Jevons ¹¹⁰, M. Jin ¹²⁵, F. Jonas ^{95,144}, P.G. Jones ¹¹⁰, J. Jung ⁶⁸, M. Jung ⁶⁸, A. Jusko ¹¹⁰, P. Kalinak ⁶⁴, A. Kalweit ³³, V. Kaplin ⁹², S. Kar ⁶, A. Karasu Uysal ⁷⁷, O. Karavichev ⁶², T. Karavicheva ⁶², P. Karczmarczyk ³³, E. Karpechev ⁶², A. Kazantsev ⁸⁷, U. Kebschull ⁷⁴, R. Keidel ⁴⁶, M. Keil ³³, B. Ketzer ⁴², Z. Khabanova ⁸⁹, A.M. Khan ⁶, S. Khan ¹⁶, S.A. Khan ¹⁴¹, A. Khanzadeev ⁹⁷, Y. Kharlov ⁹⁰, A. Khatun ¹⁶, A. Khuntia ¹¹⁸, B. Kileng ³⁵, B. Kim ⁶⁰, B. Kim ¹³³, D. Kim ¹⁴⁷, D.J. Kim ¹²⁶, E.J. Kim ⁷³, H. Kim ^{17,147}, J. Kim ¹⁴⁷, J.S. Kim ⁴⁰, J. Kim ¹⁰³, J. Kim ¹⁴⁷, J. Kim ⁷³, M. Kim ¹⁰³, S. Kim ¹⁸, T. Kim ¹⁴⁷, T. Kim ¹⁴⁷, S. Kirsch ^{38,68}, I. Kisiel ³⁸, S. Kiselev ⁹¹, A. Kisiel ¹⁴², J.L. Klay ⁵, C. Klein ⁶⁸, J. Klein ⁵⁸, S. Klein ⁷⁹, C. Klein-Bösing ¹⁴⁴, M. Kleiner ⁶⁸, A. Kluge ³³, M.L. Knichel ³³, A.G. Knospe ¹²⁵, C. Kobdaj ¹¹⁵, M.K. Köhler ¹⁰³, T. Kollegger ¹⁰⁶, A. Kondratyev ⁷⁵, N. Kondratyeva ⁹², E. Kondratyuk ⁹⁰, J. Konig ⁶⁸, P.J. Konopka ³³, L. Koska ¹¹⁶, O. Kovalenko ⁸⁴, V. Kovalenko ¹¹², M. Kowalski ¹¹⁸, I. Králik ⁶⁴, A. Kravčáková ³⁷, L. Kreis ¹⁰⁶, M. Krivda ^{64,110}, F. Krizek ⁹⁴, K. Krizkova Gajdosova ³⁶, M. Krüger ⁶⁸, E. Kryshen ⁹⁷, M. Krzewicki ³⁸, A.M. Kubera ⁹⁶, V. Kučera ⁶⁰, C. Kuhn ¹³⁶, P.G. Kuijer ⁸⁹, L. Kumar ⁹⁹, S. Kumar ⁴⁸, S. Kundu ⁸⁵, P. Kurashvili ⁸⁴, A. Kurepin ⁶², A.B. Kurepin ⁶², A. Kuryakin ¹⁰⁸, S. Kushpil ⁹⁴, J. Kvapil ¹¹⁰, M.J. Kweon ⁶⁰, J.Y. Kwon ⁶⁰, Y. Kwon ¹⁴⁷, S.L. La Pointe ³⁸, P. La Rocca ²⁷, Y.S. Lai ⁷⁹, R. Langoy ¹²⁹, K. Lapidus ³³, A. Lardeux ²⁰, P. Larionov ⁵¹, E. Laudi ³³, R. Lavicka ³⁶, T. Lazareva ¹¹², R. Lea ²⁴, L. Leardini ¹⁰³, J. Lee ¹³³, S. Lee ¹⁴⁷, F. Lehas ⁸⁹, S. Lehner ¹¹³, J. Lehrbach ³⁸, R.C. Lemmon ⁹³, I. León Monzón ¹²⁰, E.D. Lesser ¹⁹, M. Lettrich ³³, P. Lévai ¹⁴⁵, X. Li ¹², X.L. Li ⁶, J. Lien ¹²⁹, R. Lietava ¹¹⁰, B. Lim ¹⁷, V. Lindenstruth ³⁸, S.W. Lindsay ¹²⁷, C. Lippmann ¹⁰⁶, M.A. Lisa ⁹⁶, V. Litichevskyi ⁴³, A. Liu ¹⁹, S. Liu ⁹⁶, W.J. Llope ¹⁴³, I.M. Lofnes ²¹, V. Loginov ⁹², C. Loizides ⁹⁵, P. Loncar ³⁴, X. Lopez ¹³⁴, E. López Torres ⁸, J.R. Luhder ¹⁴⁴, M. Lunardon ²⁸, G. Luparello ⁵⁹, Y. Ma ³⁹, A. Maevskaya ⁶², M. Mager ³³, S.M. Mahmood ²⁰, T. Mahmoud ⁴², A. Maire ¹³⁶, R.D. Majka ¹⁴⁶, M. Malaev ⁹⁷, Q.W. Malik ²⁰, L. Malinina ^{75,iii}, D. Mal'Kevich ⁹¹, P. Malzacher ¹⁰⁶, G. Mandaglio ⁵⁵, V. Manko ⁸⁷, F. Manso ¹³⁴, V. Manzari ⁵², Y. Mao ⁶, M. Marchisone ¹³⁵, J. Mareš ⁶⁶, G.V. Margagliotti ²⁴, A. Margotti ⁵³, J. Margutti ⁶³, A. Marín ¹⁰⁶, C. Markert ¹¹⁹, M. Marquard ⁶⁸, N.A. Martin ¹⁰³, P. Martinengo ³³, J.L. Martinez ¹²⁵, M.I. Martínez ⁴⁴, G. Martínez García ¹¹⁴, M. Martinez Pedreira ³³, S. Masciocchi ¹⁰⁶, M. Masera ²⁵, A. Masoni ⁵⁴, L. Massacrier ⁶¹, E. Masson ¹¹⁴, A. Mastroserio ^{52,138},

- A.M. Mathis ^{104,117}, O. Matonoha ⁸⁰, P.F.T. Matuoka ¹²¹, A. Matyja ¹¹⁸, C. Mayer ¹¹⁸, M. Mazzilli ⁵²,
 M.A. Mazzoni ⁵⁷, A.F. Mechler ⁶⁸, F. Meddi ²², Y. Melikyan ^{62,92}, A. Menchaca-Rocha ⁷¹, C. Mengke ⁶,
 E. Meninno ^{29,113}, M. Meres ¹³, S. Mhlanga ¹²⁴, Y. Miake ¹³³, L. Micheletti ²⁵, D.L. Mihaylov ¹⁰⁴,
 K. Mikhaylov ^{75,91}, A. Mischke ^{63,i}, A.N. Mishra ⁶⁹, D. Miśkowiec ¹⁰⁶, A. Modak ³, N. Mohammadi ³³,
 A.P. Mohanty ⁶³, B. Mohanty ⁸⁵, M. Mohisin Khan ^{16,iv}, C. Mordasini ¹⁰⁴, D.A. Moreira De Godoy ¹⁴⁴,
 L.A.P. Moreno ⁴⁴, I. Morozov ⁶², A. Morsch ³³, T. Mrnjavac ³³, V. Muccifora ⁵¹, E. Mudnic ³⁴,
 D. Mühlheim ¹⁴⁴, S. Muhuri ¹⁴¹, J.D. Mulligan ⁷⁹, M.G. Munhoz ¹²¹, R.H. Munzer ⁶⁸, H. Murakami ¹³²,
 S. Murray ¹²⁴, L. Musa ³³, J. Musinsky ⁶⁴, C.J. Myers ¹²⁵, J.W. Myrcha ¹⁴², B. Naik ⁴⁸, R. Nair ⁸⁴,
 B.K. Nandi ⁴⁸, R. Nania ^{10,53}, E. Nappi ⁵², M.U. Naru ¹⁴, A.F. Nassirpour ⁸⁰, C. Nattrass ¹³⁰, R. Nayak ⁴⁸,
 T.K. Nayak ⁸⁵, S. Nazarenko ¹⁰⁸, A. Neagu ²⁰, R.A. Negrao De Oliveira ⁶⁸, L. Nellen ⁶⁹, S.V. Nesbo ³⁵,
 G. Neskovic ³⁸, D. Nesterov ¹¹², L.T. Neumann ¹⁴², B.S. Nielsen ⁸⁸, S. Nikolaev ⁸⁷, S. Nikulin ⁸⁷, V. Nikulin ⁹⁷,
 F. Noferini ^{10,53}, P. Nomokonov ⁷⁵, J. Norman ^{78,127}, N. Novitzky ¹³³, P. Nowakowski ¹⁴², A. Nyanin ⁸⁷,
 J. Nystrand ²¹, M. Ogino ⁸¹, A. Ohlson ^{80,103}, J. Oleniacz ¹⁴², A.C. Oliveira Da Silva ^{121,130}, M.H. Oliver ¹⁴⁶,
 C. Oppedisano ⁵⁸, R. Orava ⁴³, A. Ortiz Velasquez ⁶⁹, A. Oskarsson ⁸⁰, J. Otwinowski ¹¹⁸, K. Oyama ⁸¹,
 Y. Pachmayer ¹⁰³, V. Pacik ⁸⁸, D. Pagano ¹⁴⁰, G. Paić ⁶⁹, J. Pan ¹⁴³, A.K. Pandey ⁴⁸, S. Panebianco ¹³⁷,
 P. Pareek ^{49,141}, J. Park ⁶⁰, J.E. Parkkila ¹²⁶, S. Parmar ⁹⁹, S.P. Pathak ¹²⁵, R.N. Patra ¹⁴¹, B. Paul ^{23,58}, H. Pei ⁶,
 T. Peitzmann ⁶³, X. Peng ⁶, L.G. Pereira ⁷⁰, H. Pereira Da Costa ¹³⁷, D. Peresunko ⁸⁷, G.M. Perez ⁸,
 E. Perez Lezama ⁶⁸, V. Peskov ⁶⁸, Y. Pestov ⁴, V. Petráček ³⁶, M. Petrovici ⁴⁷, R.P. Pezzi ⁷⁰, S. Piano ⁵⁹,
 M. Pikna ¹³, P. Pillot ¹¹⁴, O. Pinazza ^{33,53}, L. Pinsky ¹²⁵, C. Pinto ²⁷, S. Pisano ^{10,51}, D. Pistone ⁵⁵,
 M. Płoskoń ⁷⁹, M. Planinic ⁹⁸, F. Pliquette ⁶⁸, J. Pluta ¹⁴², S. Pochybova ^{145,i}, M.G. Poghosyan ⁹⁵,
 B. Polichtchouk ⁹⁰, N. Poljak ⁹⁸, A. Pop ⁴⁷, H. Poppenborg ¹⁴⁴, S. Porteboeuf-Houssais ¹³⁴, V. Pozdniakov ⁷⁵,
 S.K. Prasad ³, R. Preghenella ⁵³, F. Prino ⁵⁸, C.A. Pruneau ¹⁴³, I. Pshenichnov ⁶², M. Puccio ^{25,33},
 J. Putschke ¹⁴³, R.E. Quishpe ¹²⁵, S. Ragoni ¹¹⁰, S. Raha ³, S. Rajput ¹⁰⁰, J. Rak ¹²⁶, A. Rakotozafindrabe ¹³⁷,
 L. Ramello ³¹, F. Rami ¹³⁶, R. Raniwala ¹⁰¹, S. Raniwala ¹⁰¹, S.S. Räsänen ⁴³, R. Rath ⁴⁹, V. Ratza ⁴²,
 I. Ravasenga ^{30,89}, K.F. Read ^{95,130}, K. Redlich ^{84,v}, A. Rehman ²¹, P. Reichelt ⁶⁸, F. Reidt ³³, X. Ren ⁶,
 R. Renfordt ⁶⁸, Z. Rescakova ³⁷, J.-P. Revol ¹⁰, K. Reygers ¹⁰³, V. Riabov ⁹⁷, T. Richert ^{80,88}, M. Richter ²⁰,
 P. Riedler ³³, W. Riegler ³³, F. Riggi ²⁷, C. Ristea ⁶⁷, S.P. Rode ⁴⁹, M. Rodríguez Cahuantzi ⁴⁴, K. Røed ²⁰,
 R. Rogalev ⁹⁰, E. Rogochaya ⁷⁵, D. Rohr ³³, D. Röhrich ²¹, P.S. Rokita ¹⁴², F. Ronchetti ⁵¹, E.D. Rosas ⁶⁹,
 K. Roslon ¹⁴², A. Rossi ^{28,56}, A. Rotondi ¹³⁹, A. Roy ⁴⁹, P. Roy ¹⁰⁹, O.V. Rueda ⁸⁰, R. Rui ²⁴, B. Rumyantsev ⁷⁵,
 A. Rustamov ⁸⁶, E. Ryabinkin ⁸⁷, Y. Ryabov ⁹⁷, A. Rybicki ¹¹⁸, H. Rytkonen ¹²⁶, O.A.M. Saarimaki ⁴³,
 S. Sadhu ¹⁴¹, S. Sadovsky ⁹⁰, K. Šafařík ³⁶, S.K. Saha ¹⁴¹, B. Sahoo ⁴⁸, P. Sahoo ^{48,49}, R. Sahoo ⁴⁹, S. Sahoo ⁶⁵,
 P.K. Sahu ⁶⁵, J. Saini ¹⁴¹, S. Sakai ¹³³, S. Sambyal ¹⁰⁰, V. Samsonov ^{92,97}, D. Sarkar ¹⁴³, N. Sarkar ¹⁴¹,
 P. Sarma ⁴¹, V.M. Sarti ¹⁰⁴, M.H.P. Sas ⁶³, E. Scapparone ⁵³, B. Schaefer ⁹⁵, J. Schambach ¹¹⁹, H.S. Scheid ⁶⁸,
 C. Schiaua ⁴⁷, R. Schicker ¹⁰³, A. Schmah ¹⁰³, C. Schmidt ¹⁰⁶, H.R. Schmidt ¹⁰², M.O. Schmidt ¹⁰³,
 M. Schmidt ¹⁰², N.V. Schmidt ^{68,95}, A.R. Schmier ¹³⁰, J. Schukraft ⁸⁸, Y. Schutz ^{33,136}, K. Schwarz ¹⁰⁶,
 K. Schweda ¹⁰⁶, G. Scioli ²⁶, E. Scomparin ⁵⁸, M. Šefčík ³⁷, J.E. Seger ¹⁵, Y. Sekiguchi ¹³², D. Sekihata ¹³²,
 I. Selyuzhenkov ^{92,106}, S. Senyukov ¹³⁶, D. Serebryakov ⁶², E. Serradilla ⁷¹, A. Sevcenco ⁶⁷, A. Shabanov ⁶²,
 A. Shabetai ¹¹⁴, R. Shahoyan ³³, W. Shaikh ¹⁰⁹, A. Shangaraev ⁹⁰, A. Sharma ⁹⁹, A. Sharma ¹⁰⁰,
 H. Sharma ¹¹⁸, M. Sharma ¹⁰⁰, N. Sharma ⁹⁹, A.I. Sheikh ¹⁴¹, K. Shigaki ⁴⁵, M. Shimomura ⁸²,
 S. Shirinkin ⁹¹, Q. Shou ³⁹, Y. Sibiriak ⁸⁷, S. Siddhanta ⁵⁴, T. Siemianczuk ⁸⁴, D. Silvermyr ⁸⁰, G. Simatovic ⁸⁹,
 G. Simonetti ^{33,104}, R. Singh ⁸⁵, R. Singh ¹⁰⁰, R. Singh ⁴⁹, V.K. Singh ¹⁴¹, V. Singhal ¹⁴¹, T. Sinha ¹⁰⁹,
 B. Sitar ¹³, M. Sitta ³¹, T.B. Skaali ²⁰, M. Slupecki ¹²⁶, N. Smirnov ¹⁴⁶, R.J.M. Snellings ⁶³,
 T.W. Snellman ^{43,126}, C. Soncco ¹¹¹, J. Song ^{60,125}, A. Songmoolnak ¹¹⁵, F. Soramel ²⁸, S. Sorensen ¹³⁰,
 I. Sputowska ¹¹⁸, J. Stachel ¹⁰³, I. Stan ⁶⁷, P. Stankus ⁹⁵, P.J. Steffanic ¹³⁰, E. Stenlund ⁸⁰, D. Stocco ¹¹⁴,
 M.M. Storetvedt ³⁵, L.D. Stritto ²⁹, A.A.P. Suade ¹²¹, T. Sugitate ⁴⁵, C. Suire ⁶¹, M. Suleymanov ¹⁴,
 M. Suljic ³³, R. Sultanov ⁹¹, M. Šumbera ⁹⁴, S. Sumowidagdo ⁵⁰, S. Swain ⁶⁵, A. Szabo ¹³, I. Szarka ¹³,
 U. Tabassam ¹⁴, G. Taillepied ¹³⁴, J. Takahashi ¹²², G.J. Tambave ²¹, S. Tang ^{6,134}, M. Tarhini ¹¹⁴,
 M.G. Tarzila ⁴⁷, A. Tauro ³³, G. Tejeda Muñoz ⁴⁴, A. Telesca ³³, C. Terrevoli ¹²⁵, D. Thakur ⁴⁹, S. Thakur ¹⁴¹,
 D. Thomas ¹¹⁹, F. Thoresen ⁸⁸, R. Tieulent ¹³⁵, A. Tikhonov ⁶², A.R. Timmins ¹²⁵, A. Toia ⁶⁸, N. Topilskaya ⁶²,
 M. Toppi ⁵¹, F. Torales-Acosta ¹⁹, S.R. Torres ^{9,120}, A. Trifiro ⁵⁵, S. Tripathy ⁴⁹, T. Tripathy ⁴⁸, S. Trogolo ²⁸,
 G. Trombetta ³², L. Tropp ³⁷, V. Trubnikov ², W.H. Trzaska ¹²⁶, T.P. Trzciński ¹⁴², B.A. Trzeciak ⁶³,
 T. Tsuji ¹³², A. Tumkin ¹⁰⁸, R. Turrisi ⁵⁶, T.S. Tveter ²⁰, K. Ullaland ²¹, E.N. Umaka ¹²⁵, A. Uras ¹³⁵,
 G.L. Usai ²³, A. Utrobiticic ⁹⁸, M. Vala ³⁷, N. Valle ¹³⁹, S. Vallero ⁵⁸, N. van der Kolk ⁶³,

L.V.R. van Doremaleen ⁶³, M. van Leeuwen ⁶³, P. Vande Vyvre ³³, D. Varga ¹⁴⁵, Z. Varga ¹⁴⁵,
 M. Varga-Kofarago ¹⁴⁵, A. Vargas ⁴⁴, M. Vasileiou ⁸³, A. Vasiliev ⁸⁷, O. Vázquez Doce ^{104,117},
 V. Vechernin ¹¹², A.M. Veen ⁶³, E. Vercellin ²⁵, S. Vergara Limón ⁴⁴, L. Vermunt ⁶³, R. Vernet ⁷,
 R. Vértesi ¹⁴⁵, L. Vickovic ³⁴, Z. Vilakazi ¹³¹, O. Villalobos Baillie ¹¹⁰, A. Villatoro Tello ⁴⁴, G. Vino ⁵²,
 A. Vinogradov ⁸⁷, T. Virgili ²⁹, V. Vislavicius ⁸⁸, A. Vodopyanov ⁷⁵, B. Volkel ³³, M.A. Völkl ¹⁰²,
 K. Voloshin ⁹¹, S.A. Voloshin ¹⁴³, G. Volpe ³², B. von Haller ³³, I. Vorobyev ¹⁰⁴, D. Voscek ¹¹⁶, J. Vrláková ³⁷,
 B. Wagner ²¹, M. Weber ¹¹³, S.G. Weber ¹⁴⁴, A. Wegrzynek ³³, D.F. Weiser ¹⁰³, S.C. Wenzel ³³,
 J.P. Wessels ¹⁴⁴, J. Wiechula ⁶⁸, J. Wikne ²⁰, G. Wilk ⁸⁴, J. Wilkinson ^{10,53}, G.A. Willems ³³, E. Willsher ¹¹⁰,
 B. Windelband ¹⁰³, M. Winn ¹³⁷, W.E. Witt ¹³⁰, Y. Wu ¹²⁸, R. Xu ⁶, S. Yalcin ⁷⁷, K. Yamakawa ⁴⁵, S. Yang ²¹,
 S. Yano ¹³⁷, Z. Yin ⁶, H. Yokoyama ⁶³, I.-K. Yoo ¹⁷, J.H. Yoon ⁶⁰, S. Yuan ²¹, A. Yuncu ¹⁰³, V. Yurchenko ²,
 V. Zaccole ²⁴, A. Zaman ¹⁴, C. Zampolli ³³, H.J.C. Zanolli ⁶³, N. Zardoshti ³³, A. Zarochentsev ¹¹²,
 P. Závada ⁶⁶, N. Zaviyalov ¹⁰⁸, H. Zbroszczyk ¹⁴², M. Zhalov ⁹⁷, S. Zhang ³⁹, X. Zhang ⁶, Z. Zhang ⁶,
 V. Zhrebchevskii ¹¹², D. Zhou ⁶, Y. Zhou ⁸⁸, Z. Zhou ²¹, J. Zhu ^{6,106}, Y. Zhu ⁶, A. Zichichi ^{10,26},
 M.B. Zimmermann ³³, G. Zinovjev ², N. Zurlo ¹⁴⁰

¹ A.I. Alikhanian National Science Laboratory (Yerevan Physics Institute) Foundation, Yerevan, Armenia² Bogolyubov Institute for Theoretical Physics, National Academy of Sciences of Ukraine, Kiev, Ukraine³ Bose Institute, Department of Physics and Centre for Astroparticle Physics and Space Science (CAPSS), Kolkata, India⁴ Budker Institute for Nuclear Physics, Novosibirsk, Russia⁵ California Polytechnic State University, San Luis Obispo, CA, United States⁶ Central China Normal University, Wuhan, China⁷ Centre de Calcul de l'IN2P3, Villeurbanne, Lyon, France⁸ Centro de Aplicaciones Tecnológicas y Desarrollo Nuclear (CEADEN), Havana, Cuba⁹ Centro de Investigación y de Estudios Avanzados (CINVESTAV), Mexico City and Mérida, Mexico¹⁰ Centro Fermi – Museo Storico della Fisica e Centro Studi e Ricerche "Enrico Fermi", Rome, Italy¹¹ Chicago State University, Chicago, IL, United States¹² China Institute of Atomic Energy, Beijing, China¹³ Comenius University Bratislava, Faculty of Mathematics, Physics and Informatics, Bratislava, Slovakia¹⁴ COMSATS University Islamabad, Islamabad, Pakistan¹⁵ Creighton University, Omaha, NE, United States¹⁶ Department of Physics, Aligarh Muslim University, Aligarh, India¹⁷ Department of Physics, Pusan National University, Pusan, Republic of Korea¹⁸ Department of Physics, Sejong University, Seoul, Republic of Korea¹⁹ Department of Physics, University of California, Berkeley, CA, United States²⁰ Department of Physics, University of Oslo, Oslo, Norway²¹ Department of Physics and Technology, University of Bergen, Bergen, Norway²² Dipartimento di Fisica dell'Università 'La Sapienza' and Sezione INFN, Rome, Italy²³ Dipartimento di Fisica dell'Università and Sezione INFN, Cagliari, Italy²⁴ Dipartimento di Fisica dell'Università and Sezione INFN, Trieste, Italy²⁵ Dipartimento di Fisica dell'Università and Sezione INFN, Turin, Italy²⁶ Dipartimento di Fisica e Astronomia dell'Università and Sezione INFN, Bologna, Italy²⁷ Dipartimento di Fisica e Astronomia dell'Università and Sezione INFN, Catania, Italy²⁸ Dipartimento di Fisica e Astronomia dell'Università and Sezione INFN, Padova, Italy²⁹ Dipartimento di Fisica 'E.R. Caianiello' dell'Università and Gruppo Collegato INFN, Salerno, Italy³⁰ Dipartimento DISAT del Politecnico and Sezione INFN, Turin, Italy³¹ Dipartimento di Scienze e Innovazione Tecnologica dell'Università del Piemonte Orientale and INFN Sezione di Torino, Alessandria, Italy³² Dipartimento Interateneo di Fisica 'M. Merlin' and Sezione INFN, Bari, Italy³³ European Organization for Nuclear Research (CERN), Geneva, Switzerland³⁴ Faculty of Electrical Engineering, Mechanical Engineering and Naval Architecture, University of Split, Split, Croatia³⁵ Faculty of Engineering and Science, Western Norway University of Applied Sciences, Bergen, Norway³⁶ Faculty of Nuclear Sciences and Physical Engineering, Czech Technical University in Prague, Prague, Czech Republic³⁷ Faculty of Science, P.J. Šafárik University, Košice, Slovakia³⁸ Frankfurt Institute for Advanced Studies, Johann Wolfgang Goethe-Universität Frankfurt, Frankfurt, Germany³⁹ Fudan University, Shanghai, China⁴⁰ Gangneung-Wonju National University, Gangneung, Republic of Korea⁴¹ Gauhati University, Department of Physics, Guwahati, India⁴² Helmholtz-Institut für Strahlen- und Kernphysik, Rheinische Friedrich-Wilhelms-Universität Bonn, Bonn, Germany⁴³ Helsinki Institute of Physics (HIP), Helsinki, Finland⁴⁴ High Energy Physics Group, Universidad Autónoma de Puebla, Puebla, Mexico⁴⁵ Hiroshima University, Hiroshima, Japan⁴⁶ Hochschule Worms, Zentrum für Technologietransfer und Telekommunikation (ZTT), Worms, Germany⁴⁷ Horia Hulubei National Institute of Physics and Nuclear Engineering, Bucharest, Romania⁴⁸ Indian Institute of Technology Bombay (IIT), Mumbai, India⁴⁹ Indian Institute of Technology Indore, Indore, India⁵⁰ Indonesian Institute of Sciences, Jakarta, Indonesia⁵¹ INFN, Laboratori Nazionali di Frascati, Frascati, Italy⁵² INFN, Sezione di Bari, Bari, Italy⁵³ INFN, Sezione di Bologna, Bologna, Italy⁵⁴ INFN, Sezione di Cagliari, Cagliari, Italy⁵⁵ INFN, Sezione di Catania, Catania, Italy⁵⁶ INFN, Sezione di Padova, Padova, Italy⁵⁷ INFN, Sezione di Roma, Rome, Italy⁵⁸ INFN, Sezione di Torino, Turin, Italy

- ⁵⁹ INFN, Sezione di Trieste, Trieste, Italy
⁶⁰ Inha University, Incheon, Republic of Korea
⁶¹ Institut de Physique Nucléaire d'Orsay (IPNO), Institut National de Physique Nucléaire et de Physique des Particules (IN2P3/CNRS), Université de Paris-Sud, Université Paris-Saclay, Orsay, France
⁶² Institute for Nuclear Research, Academy of Sciences, Moscow, Russia
⁶³ Institute for Subatomic Physics, Utrecht University/Nikhef, Utrecht, Netherlands
⁶⁴ Institute of Experimental Physics, Slovak Academy of Sciences, Košice, Slovakia
⁶⁵ Institute of Physics, Homi Bhabha National Institute, Bhubaneswar, India
⁶⁶ Institute of Physics of the Czech Academy of Sciences, Prague, Czech Republic
⁶⁷ Institute of Space Science (ISS), Bucharest, Romania
⁶⁸ Institut für Kernphysik, Johann Wolfgang Goethe-Universität Frankfurt, Frankfurt, Germany
⁶⁹ Instituto de Ciencias Nucleares, Universidad Nacional Autónoma de México, Mexico City, Mexico
⁷⁰ Instituto de Física, Universidade Federal do Rio Grande do Sul (UFRGS), Porto Alegre, Brazil
⁷¹ Instituto de Física, Universidad Nacional Autónoma de México, Mexico City, Mexico
⁷² iThemba LABS, National Research Foundation, Somerset West, South Africa
⁷³ Jeonbuk National University, Jeonju, Republic of Korea
⁷⁴ Johann-Wolfgang-Goethe Universität Frankfurt Institut für Informatik, Fachbereich Informatik und Mathematik, Frankfurt, Germany
⁷⁵ Joint Institute for Nuclear Research (JINR), Dubna, Russia
⁷⁶ Korea Institute of Science and Technology Information, Daejeon, Republic of Korea
⁷⁷ KTO Karatay University, Konya, Turkey
⁷⁸ Laboratoire de Physique Subatomique et de Cosmologie, Université Grenoble-Alpes, CNRS-IN2P3, Grenoble, France
⁷⁹ Lawrence Berkeley National Laboratory, Berkeley, CA, United States
⁸⁰ Lund University Department of Physics, Division of Particle Physics, Lund, Sweden
⁸¹ Nagasaki Institute of Applied Science, Nagasaki, Japan
⁸² Nara Women's University (NWU), Nara, Japan
⁸³ National and Kapodistrian University of Athens, School of Science, Department of Physics, Athens, Greece
⁸⁴ National Centre for Nuclear Research, Warsaw, Poland
⁸⁵ National Institute of Science Education and Research, Homi Bhabha National Institute, Jatni, India
⁸⁶ National Nuclear Research Center, Baku, Azerbaijan
⁸⁷ National Research Centre Kurchatov Institute, Moscow, Russia
⁸⁸ Niels Bohr Institute, University of Copenhagen, Copenhagen, Denmark
⁸⁹ Nikhef, National institute for subatomic physics, Amsterdam, Netherlands
⁹⁰ NRC Kurchatov Institute IHEP, Protvino, Russia
⁹¹ NRC "Kurchatov Institute" – ITEP, Moscow, Russia
⁹² NRNU Moscow Engineering Physics Institute, Moscow, Russia
⁹³ Nuclear Physics Group, STFC Daresbury Laboratory, Daresbury, United Kingdom
⁹⁴ Nuclear Physics Institute of the Czech Academy of Sciences, Řež u Prahy, Czech Republic
⁹⁵ Oak Ridge National Laboratory, Oak Ridge, TN, United States
⁹⁶ Ohio State University, Columbus, OH, United States
⁹⁷ Petersburg Nuclear Physics Institute, Gatchina, Russia
⁹⁸ Physics department, Faculty of science, University of Zagreb, Zagreb, Croatia
⁹⁹ Physics Department, Panjab University, Chandigarh, India
¹⁰⁰ Physics Department, University of Jammu, Jammu, India
¹⁰¹ Physics Department, University of Rajasthan, Jaipur, India
¹⁰² Physikalisches Institut, Eberhard-Karls-Universität Tübingen, Tübingen, Germany
¹⁰³ Physikalisches Institut, Ruprecht-Karls-Universität Heidelberg, Heidelberg, Germany
¹⁰⁴ Physik Department, Technische Universität München, Munich, Germany
¹⁰⁵ Politecnico di Bari, Bari, Italy
¹⁰⁶ Research Division and ExtreMe Matter Institute EMMI, GSI Helmholtzzentrum für Schwerionenforschung GmbH, Darmstadt, Germany
¹⁰⁷ Rudjer Bošković Institute, Zagreb, Croatia
¹⁰⁸ Russian Federal Nuclear Center (VNIIEF), Sarov, Russia
¹⁰⁹ Saha Institute of Nuclear Physics, Homi Bhabha National Institute, Kolkata, India
¹¹⁰ School of Physics and Astronomy, University of Birmingham, Birmingham, United Kingdom
¹¹¹ Sección Física, Departamento de Ciencias, Pontificia Universidad Católica del Perú, Lima, Peru
¹¹² St. Petersburg State University, St. Petersburg, Russia
¹¹³ Stefan Meyer Institut für Subatomare Physik (SMI), Vienna, Austria
¹¹⁴ SUBATECH, IMT Atlantique, Université de Nantes, CNRS-IN2P3, Nantes, France
¹¹⁵ Suranaree University of Technology, Nakhon Ratchasima, Thailand
¹¹⁶ Technical University of Košice, Košice, Slovakia
¹¹⁷ Technische Universität München, Excellence Cluster 'Universe', Munich, Germany
¹¹⁸ The Henryk Niewodniczanski Institute of Nuclear Physics, Polish Academy of Sciences, Cracow, Poland
¹¹⁹ The University of Texas at Austin, Austin, TX, United States
¹²⁰ Universidad Autónoma de Sinaloa, Culiacán, Mexico
¹²¹ Universidade de São Paulo (USP), São Paulo, Brazil
¹²² Universidade Estadual de Campinas (UNICAMP), Campinas, Brazil
¹²³ Universidade Federal do ABC, Santo André, Brazil
¹²⁴ University of Cape Town, Cape Town, South Africa
¹²⁵ University of Houston, Houston, TX, United States
¹²⁶ University of Jyväskylä, Jyväskylä, Finland
¹²⁷ University of Liverpool, Liverpool, United Kingdom
¹²⁸ University of Science and Technology of China, Hefei, China
¹²⁹ University of South-Eastern Norway, Tønsberg, Norway
¹³⁰ University of Tennessee, Knoxville, TN, United States
¹³¹ University of the Witwatersrand, Johannesburg, South Africa
¹³² University of Tokyo, Tokyo, Japan
¹³³ University of Tsukuba, Tsukuba, Japan
¹³⁴ Université Clermont Auvergne, CNRS/IN2P3, LPC, Clermont-Ferrand, France
¹³⁵ Université de Lyon, Université Lyon 1, CNRS/IN2P3, IPN-Lyon, Villeurbanne, Lyon, France
¹³⁶ Université de Strasbourg, CNRS, IPHC UMR 7178, F-67000 Strasbourg, France
¹³⁷ Université Paris-Saclay Centre d'Etudes de Saclay (CEA), IRFU, Département de Physique Nucléaire (DPhN), Saclay, France

¹³⁸ Università degli Studi di Foggia, Foggia, Italy

¹³⁹ Università degli Studi di Pavia, Pavia, Italy

¹⁴⁰ Università di Brescia, Brescia, Italy

¹⁴¹ Variable Energy Cyclotron Centre, Homi Bhabha National Institute, Kolkata, India

¹⁴² Warsaw University of Technology, Warsaw, Poland

¹⁴³ Wayne State University, Detroit, MI, United States

¹⁴⁴ Westfälische Wilhelms-Universität Münster, Institut für Kernphysik, Münster, Germany

¹⁴⁵ Wigner Research Centre for Physics, Budapest, Hungary

¹⁴⁶ Yale University, New Haven, CT, United States

¹⁴⁷ Yonsei University, Seoul, Republic of Korea

ⁱ Deceased.

ⁱⁱ Dipartimento DET del Politecnico di Torino, Turin, Italy.

ⁱⁱⁱ M.V. Lomonosov Moscow State University, D.V. Skobeltsyn Institute of Nuclear, Physics, Moscow, Russia.

^{iv} Department of Applied Physics, Aligarh Muslim University, Aligarh, India.

^v Institute of Theoretical Physics, University of Wroclaw, Poland.